

THESIS

DESIGN OF AN INHALABLE AEROSOL SIZE SPECTROMETER

Submitted by

Mwangi Ndonga

Department of Environmental and Radiological Health Sciences

In partial fulfillment of the requirements

For the Degree of Master of Science

Colorado State University

Fort Collins, Colorado

Spring 2015

Master's Committee:

Advisor: John Volckens

Stephen Reynolds
Sonia Kreidenweis

Copyright by Mwangi Ndonga 2015

All Rights Reserved

ABSTRACT

DESIGN OF AN INHALABLE AEROSOL SIZE SPECTROMETER

Industrial hygienists lack the proper instruments to measure size distributions of inhalable particulate matter (0-100 μm) as defined by ACGIH/ISO/CEN. The Portable Inhalable Particle Spectrometer (PIPS) was designed to size-segregate IPM in calm-air environments – which constitute a majority of workplaces. The PIPS uses an upward air velocity to restrict particle aspiration into the device to diameters above a specified cut-size. A vertical test chamber was also designed to facilitate aerosol dispersion and experimental evaluation of the PIPS. Two PIPS tubes were tested (1.5 cm and 5 cm) at four face velocities (0.6, 1.35, 2.5 and 3.5 $\text{cm}\cdot\text{s}^{-1}$) that correspond to cut-sizes of 20, 30, 40 and 50 μm in aerodynamic diameter, respectively. The observed performance of the PIPS deviated from model estimates as face velocity or tube diameter was increased. The fluid regime present inside the chamber, due to the operating PIPS, likely influenced the measured sampling efficiency of the PIPS.

ACKNOWLEDGMENTS

This research was conducted with financial support from the Mountain and Plains Educational Research Center and High Plains Intermountain Center for Agricultural Health and Safety.

TABLE OF CONTENTS

ABSTRACT.....	ii
ACKNOWLEDGMENTS.....	iii
NOMENCLATURE	vi
1. Introduction.....	1
1.1. Occupational Respiratory Diseases	1
1.2. The Benefits of Measuring Particle Size Distribution	1
1.3. Aerosol Samplers.....	3
1.3.1 Personal Inhalable Samplers	3
1.3.2 Samplers for Measuring Size Distributions.....	4
1.4. Aerosol Inhalability	5
1.5. The Exclusion of Large Inhalable Particles in Health Assessments.....	6
1.6. Calm Air Sampling.....	6
1.7. The Need for a Size-Resolved Sampler for Inhalable Dust Size Distributions	8
2. Research Aims	9
3. PIPS and Test Chamber Design.....	10
3.1. Portable Inhalable Particle Spectrometer (PIPS) Design.....	10
3.1.1. Particle Settling	10
3.1.2. Laminar Flow in a PIPS Tube	12
3.1.3. Particle Settling in a PIPS Tube	15
3.1.4. Collection and Rejection Errors Due to Developing Laminar Flow	16
3.1.5. PIPS Tube Characteristics.....	19
3.1.6. Fluid flow assumptions	20
3.2. Test chamber.....	20
4. Experimental Method.....	23
4.1 Verification of a Calm-air Environment.....	23
4.2 Preparing Aerosol	23
4.3 Particle Deposition on the Chamber Floor	23
4.4 Dispersion of polyethylene spheres	24
4.5. Regulating PIPS Flow and Placement of Control filters	25
4.6. Aerosol Generation.....	26
4.7. Collection of Sampling Media.....	26
4.8. Experimental Conditions	27
4.9. Measurement of Sampling Efficiency	27
4.10. Fluorescent Microscopy	29
4.11. Tube efficiency	30
5. Results and Discussion	31

5.1 Size Distribution of Test Aerosol	31
5.2. Mixing of Test Aerosol.....	32
5.3 Calm-air environment.....	33
5.4. Sampling Efficiency	34
5.5 PIPS tube for 20 μm cut-size.....	34
5.6 PIPS tube for 30 μm cut-size.....	36
5.7 PIPS tube for 40 μm cut-size.....	38
5.8 PIPS tube for 50 μm cut-size.....	39
5.9 Sampling efficiencies for particle size bins	41
5.10 PIPS velocity and chamber deposition	42
5.11 Fluid flow assumptions.....	46
6. Conclusions and Suggested Future Work.....	47
7. References.....	50
APPENDIX.....	53

NOMENCLATURE

C_c	Cunningham correction factor
CV_T	Total coefficient of variation of PIPS and control filters
CV_{PIPS}	Coefficient of variation of particle counts for the PIPS filter
$CV_{controls}$	Coefficient of variation of particle counts for the control filters
d_p	Particle diameter
$d_{20\%}$	Particle diameter corresponding to 20% sampling efficiency
$d_{50\%}$	Particle diameter corresponding to 50% sampling efficiency
$d_{80\%}$	Particle diameter corresponding to 80% sampling efficiency
F_d	Force due to drag
F_g	Force due to gravity
L_E	Entrance length
$\bar{N}_{PIPS,i}$	Average number of particles of the i^{th} size on the PIPS filter
$\bar{N}_{control,i}$	Average number of particles of the i^{th} size on the control filter
Q_0	Initial tube volumetric flowrate
Re_f	Fluid Reynolds number
U_y	Dimensionless axial velocity
V_{ts}	Particle settling velocity
$V_{y,0}$	Y-axial component of initial tube velocity
$V_{y,radial}$	Y-axial component of radial velocity
x	Distance in the x-direction between tube wall and tube radius
α	Dimensionless radius of the inviscid core
ρ_p	Density of particle

ρ_g	Density of gas
λ	Mean free path
$\eta_{mod,i}$	Modeled tube sampling efficiency for the i^{th} size
$\eta_{meas,i}$	Measured tube sampling efficiency for the i^{th} size
$\bar{\eta}_{mod}$	Modeled mean sampling efficiency
$\bar{\eta}_{meas}$	Measured mean sampling efficiency
ϕ	Dimensionless axial velocity of the inviscid core

1. Introduction

1.1. Occupational Respiratory Diseases

Thousands of new cases of respiratory diseases (e.g., silicosis, pneumoconiosis, bronchitis, asthma, rhinitis and COPD) caused by occupational aerosol exposure continue to appear on a yearly basis¹. Workers encounter hazardous aerosols in mining, construction, oil and gas extraction, agriculture, forestry and fishing. Such aerosols include wood dust, metalworking fluid, crystalline silica, coal dust, pesticides, diesel particulate matter, and asbestos, as examples²⁻¹⁰. The National Institute of Occupational Safety and Health (NIOSH) has identified gaps in our ability to measure, control, and evaluate aerosol exposures for the study and prevention of these etiological agents¹¹. These gaps hinder our ability to protect against the incidence of occupational respiratory disease. Effective aerosol measurement is the most consequential of the research gaps – accurate and representative hazard characterization is the foundation for the design of controls and exposure assessments.

1.2. The Benefits of Measuring Particle Size Distribution

The measurement of aerosol size distribution allows for the prediction of particle deposition in the human respiratory system and aids in the determination of aerosol source and transport in the workplace. Particle size measurement also provides a basis for the characterization of hazardous work environments, design of ventilation systems and assignment of personal protective equipment¹².

Inhalation is the mechanism by which aerosols enter the respiratory system¹³. The American Conference of Governmental Industrial Hygienists (ACGIH) defines inhalable particle matter (IPM) as those materials that are hazardous when deposited anywhere in the respiratory tract and as having diameters (d_p) between 0-100 μm ¹⁴. Particle size, more than any other particle property, governs the transport and deposition of inhalable particles in the three regions (oronasal, tracheobronchial, and pulmonary) of the human respiratory system¹². The oronasal region contains the nose, mouth, nasopharynx, oropharynx, laryngopharynx; particles with $d_p < 100 \mu\text{m}$ may enter and deposit in this region. The tracheobronchial region contains the trachea, bronchi and bronchioles (to terminal bronchioles); particles with $d_p < 25 \mu\text{m}$ may enter and deposit in this region. The pulmonary region contains the respiratory bronchioles, alveolar ducts, alveolar sacs and alveoli; particles with $d_p < 10 \mu\text{m}$ may enter and deposit in this region. The oronasal, tracheobronchial and pulmonary regions are labeled as ‘inhalable’, ‘thoracic’ and ‘respirable’, respectively, by ACGIH. Thus, given a dust size distribution, an industrial hygienist can classify particulate matter (PM) hazards as inhalable, thoracic or respirable.

Particle type (metallic, biologic, etc.) and method of generation (abrasion, condensation, etc.) may also be inferred from particle size distributions¹³. For example, vapor condensation or combustion processes yield primarily sub-micron particles ($d_p < 1 \mu\text{m}$) and mechanical, abrasive processes yield primarily super-micron particles ($d_p > 1 \mu\text{m}$). Dusts that are re-suspended from floors and surfaces often extend well into the IPM range.

1.3. Aerosol Samplers

Sampling challenges that hinder the industrial hygienist from properly measuring IPM size distributions are: inadequate sampling methodology (e.g. total dust sampling) and improperly designed samplers.

1.3.1 Personal Inhalable Samplers

The most widely used sampling method for particles/dust is “total dust” sampling. With this type of sampling the sampling time, sampler flow rate, and change in filter mass (gravimetric analysis) are used to determine dust concentration. The label “total dust sampler” is a misnomer. In operation, total dust samplers (and virtually all aerosol samplers) are limited in their ability to sample aerosol. Two measures of efficiency are of interest when evaluating the performance of inhalable aerosol samplers. First, aspiration efficiency is the efficiency with which particles are transported from the ambient air into the inlet of the sampler¹⁵. Second, sampling or collection efficiency is the efficiency with which particles are collected on a medium downstream of the sampler inlet relative to an ambient particle concentration. Particle transmission loss may contribute to the difference in aspiration and collection efficiencies¹⁶.

The most widely used personal sampler in the U.S. for industrial hygiene sampling is the 37-mm cassette¹⁷. The 37-mm cassette, which is incorrectly labeled as a ‘total dust sampler’, allows for the collection of particles in both an open and closed configuration. Other samplers such as the IOM (Institute of Medicine) or Button (SKC) samplers are – in design – an improvement to the 37-mm cassette¹⁸. The Button sampler, for example, has a mesh screen designed to keep very large particles ($d_p > 100 \mu\text{m}$) from being collected. Outside North America, the IOM sampler is considered the standard for IPM sampling. Research has shown that the orientation-averaged sampling efficiency of the IOM to be in close agreement with the

inhalable sampling criterion for IPM at low windspeeds. However, all three samplers have been shown to both underestimate and overestimate particle concentration under various conditions¹⁵⁻¹⁷.

Overall, personal samplers have the same limitation: they do not report size distribution. Measurement of particle size distribution, not mass concentration, helps predict where particles may lodge in the respiratory tract and how best to control them at their source¹².

1.3.2 Samplers for Measuring Size Distributions

Instruments that measure size distributions such as impactors, elutriators, light scattering devices and the Personal Inhalable Dust Spectrometer (PIDS) are moderately useful in the assessment of IPM hazards¹⁰. The range of measurement of each type of instrument is limited to specific segments of the inhalable criterion (Figure 1) put forth by ACGIH, the International Standards Organization (ISO) and the European Comité Européen de Normalisation (CEN) – the basis for the criterion is described in the following section. No single instrument is useful in reporting particle size distributions that contain particles with $d_p > 20 \mu\text{m}$.

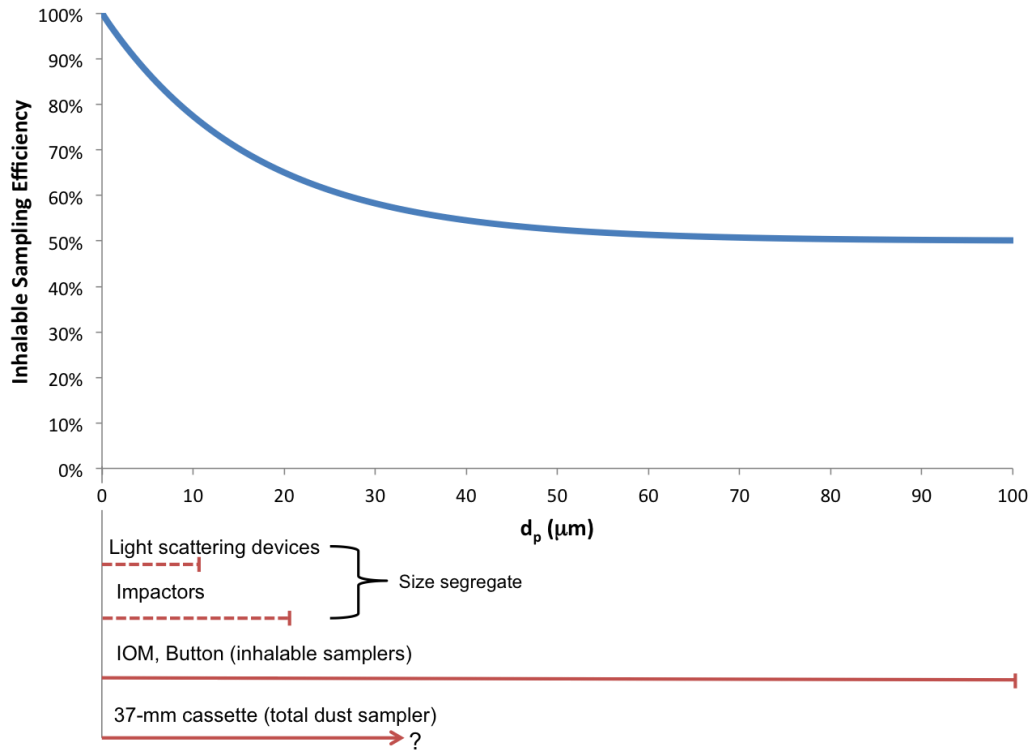


Figure 1: The ACGIH/ISO/CEN criteria for inhalable aerosol and size limitations of aerosol measuring instruments.

1.4. Aerosol Inhalability

The inhalable convention endorsed by ACGIH, ISO and CEN (Figure 1) is an elementary means of describing human aspiration of inhalable particles. The curve in Figure 1 also defines the desired aspiration efficiency of an aerosol sampler (to mimic human inhalation) as a function of particle size up to $100 \mu\text{m}$ ¹³. The ACGIH/ISO/CEN criterion proceeded from studies of particle aspiration efficiency into and through the oronasal region of head manikins at low wind speeds ($0.5 \text{ m}\cdot\text{s}^{-1}$ to $4 \text{ m}\cdot\text{s}^{-1}$)¹². According to the ACGIH inhalable convention, smaller particles ($d_p < 10 \mu\text{m}$) are inhaled at almost 100% efficiency and larger particles ($10 < d_p < 100 \mu\text{m}$) are inhaled at a gradually decreasing efficiency down to 50%¹⁴. Importantly, the ACGIH/ISO/CEN convention cannot accurately reflect the fraction of particles deposited in the respiratory tract region of interest, as the deposition depends on worker-related (work rate, worker fitness, nose

vs. mouth breathing, etc.) and workplace-related (air speed and direction, proximity to source, etc.) parameters¹⁹. However, this curve is considered a conservative model of inhalation risk, since many inhaled particles may also be exhaled.

The ACGIH/ISO/CEN inhalable criterion was developed and validated at moderately-high windspeed value ($0.5 \text{ m}\cdot\text{s}^{-1}$ to $4 \text{ m}\cdot\text{s}^{-1}$). These windspeeds are representative of those reported in coal mines and in outdoor environments. At very high wind speeds (above $4 \text{ m}\cdot\text{s}^{-1}$), an increase in aspiration efficiency is observed for $20 < d_p < 100 \text{ }\mu\text{m}$, rendering the ACGIH/ISO/CEN inhalable criterion unsuitable for such conditions¹². The ACGIH/ISO/CEN criterion is also unsuitable for calm-air environments, which actually constitute the majority of workplaces. Baldwin and Maynard (1998) showed that air velocities (forced ventilation or naturally occurring) in typical indoor workplaces range from $0.1 \text{ m}\cdot\text{s}^{-1}$ to $0.3 \text{ m}\cdot\text{s}^{-1}$ - much lower than the range used to develop the ACGIH/ISO/CEN curve²⁰. These and other observations indicate that new conventions for dust inhalability in calm-air environments are needed¹⁹.

1.5. The Exclusion of Large Inhalable Particles in Health Assessments

Often, large particles are ignored in health assessments because they are far more likely to settle before being inhaled. However, during mechanical breakup of solid materials (wood, concrete, metal) particles become airborne and, if within the vicinity of a worker, are likely to be inhaled²². Settled particles may also be resuspended due to human and/or environmental influences (e.g., wind, movement, etc.).

1.6. Calm Air Sampling

Progress towards a better understanding of inhalable aerosol sampling in calm-air has been slowed because of an historic paradigm that calls for sampler testing in wind tunnels. Yet,

only one aerosol test facility, in the literature, has been successfully operated at wind speeds as low as $0.1 \text{ m}\cdot\text{s}^{-1}$ ^{21,22}. As an alternative to wind-tunnel testing, recent studies of large aerosol behavior in calm air have employed vertical settling chambers. A vertical chamber can accommodate gravitational settling of larger particles better than a horizontal wind tunnel operated at very low wind-speed ^{18,23,24}.

Aitken et al. (1999) devised an experimental system to evaluate oral aspiration efficiency of a manikin for a range of particles (6-90 μm) and breathing patterns (rest, moderate work, and heavy work). The manikin was fitted with IOM, seven-hole and closed-face 37-mm cassette samplers, and housed in a vertical chamber 3 m in height. Their results showed that, generally, inhalation aspiration efficiency in calm air was higher compared to the efficiencies of the ACGIH/ISO/CEN curve ²³.

A similar study was conducted by Hsu and Swift (1999) using adult and child manikins and two breathing conditions (rest, moderate work). Results for an adult manikin undergoing nasal breathing at rest indicated that particles larger than 110 μm had zero aspiration efficiency in calm air; particles in the range of 110-135 μm had small aspiration efficiencies when breathing rate was increased to represent moderate exercise. They conclude 110 μm to be the cutoff particle size for nasal aspiration. This conclusion differs substantially from Aitken et al. (1999) and from the ACGIH/ISO/CEN convention – which states that particles on the order of $d_p \approx 100 \mu\text{m}$ are inhaled at 50% efficiency ²⁴.

1.7. The Need for a Size-Resolved Sampler for Inhalable Dust Size Distributions

In occupational settings, the industrial hygienist lacks the proper technology to measure inhalable dust size distributions. Despite a wide-array of aerosol measurement devices available, few (if any) devices are capable of measuring size distributions accurately above 20 μm – significantly below the upper limit of the ACGIH/ISO/CEN criterion¹⁹. Yet, aerosols with $d_p > 20$ μm such as organic dusts, pollen, mists, fly ash, paint spray, cement dust are prevalent in indoor and outdoor occupational environments. Furthermore, the design of industrial hygiene controls, conduction of exposure assessments and retrospective epidemiological studies are hindered by this lack of technology. Currently, there is no published work describing a device capable of reporting inhalable size distributions in calm-air environments. Therefore, a need exists for an instrument that characterizes inhalable particle size distributions in occupational settings such as agriculture, forestry, construction and mining where inhalable aerosols pose significant health hazards²⁻¹⁰.

2. Research Aims

This research has two aims. The first aim is to design and characterize a two-stage vertical chamber to simulate inhalable dust behavior in calm-air. The second aim is to design and test a Portable Inhalable Particle Spectrometer (PIPS) that will segregate inhalable aerosol into pre-defined size ranges.

3. PIPS and Test Chamber Design

3.1. Portable Inhalable Particle Spectrometer (PIPS) Design

The design principle of the PIPS is similar to that of a horizontal elutriator operated in a vertical orientation. A PIPS tube uses an upward velocity of air to restrict aerosol aspiration into the device to particle diameters above a specified cut-size. The aspirated aerosol deposits on a filter (Cellulose Support Pad, Pall) at the bottom of the tube.

The following sections describe the design approach for a PIPS. The approach is prefaced by an explanation of the expected fluid flow/regime within a PIPS tube. Particle settling theory and fluid dynamics provide a basis for the design and modeled performance for a PIPS.

3.1.1. Particle Settling

A particle settling through a fluid reaches its terminal settling velocity (V_{ts}) when the upward drag of the fluid equals the downward force of gravity (Figure 2)¹³.

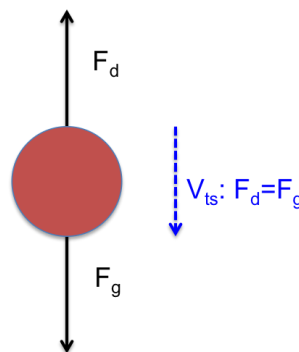


Figure 2: Forces on a settling particle. Terminal velocity occurs when the fluid drag force equals the force due to gravity.

The particle's velocity will remain constant at its V_{ts} during settling, provided the surrounding air environment is calm. A spherical particle settling under laminar flow (i.e., Stokes flow) is determined from several physical parameters,

$$V_{ts} = \frac{d_p^2 g r_p C_c}{18\mu} \quad (1)$$

where d_p is the particle diameter, g is the acceleration due to gravity, ρ_p is the particle density, C_c is the Cunningham correction factor and μ is the fluid viscosity. The Cunningham correction factor accounts for the effect of particle slip under Stokes' law and is obtained using Equation 2.

$$C_c = 1 + \frac{\lambda}{d_p} \left(2.34 + 1.05 \exp\left(-\frac{d_p}{\lambda}\right) - 0.39 \frac{\lambda}{d_p} \right) \quad (2)$$

where λ is the mean free path. When $d_p > 3 \mu\text{m}$, $C_c \approx 1$. For particle settling outside the Stokes' drag region (when particle Reynolds number ($Re_p > 1$), V_{ts} cannot be obtained explicitly from Eq. 1. Instead, an alternative approach, that is accurate within 3% for $1 < Re_p < 600$, is used. The corrected V_{ts} is

$$V_{ts} = \left(\frac{\mu}{\rho_g d_p} \right) \exp(-3.070 + 0.9935J - 0.0178J^2) \quad (3)$$

where

$$J = \ln \left(\frac{4 r_p r_g d_p^3 g}{3 \mu^2} \right) \quad (4)$$

and ρ_g is the gas density.

When a particle settles near the aspirating head of a PIPS tube, its behavior is largely dependent on V_{ts} . If the upward velocity of air (V_y) through the tube is greater in magnitude than V_{ts} , then the air will force the particle upward and away from the inlet (rejection). If $V_y < V_{ts}$, then the particle will theoretically enter the tube and settle onto the filter (collection). Overall, collection and rejection by each PIPS tube is modeled under this principle.

3.1.2. Laminar Flow in a PIPS Tube

Fully developed laminar flow retains a stable, parabolic velocity profile as it traverses a pipe. However, closer to the flow inlet there is a region in which the presence of a growing boundary layer yields a non-parabolic flow profile (Figure 3). This fluid phenomenon is a result of surface friction, fluid viscosity, and conservation of mass/momentum. For incompressible flow, mass conservation requires that, as the fluid velocity close to the wall is reduced by friction, the velocity away from the wall (in the central frictionless, or inviscid, region) must increase to compensate. This phenomenon results in the characteristic parabolic shape of laminar flow in a pipe. After a certain length, known as the entrance length (L_E), the parabolic profile will cease changing shape. The entrance length is

$$L_E \gg 0.06DRe_f \quad (\text{Laminar flow}) \quad (5)$$

Beyond that length, the flow is considered fully developed and maintains the same parabolic shape downstream.

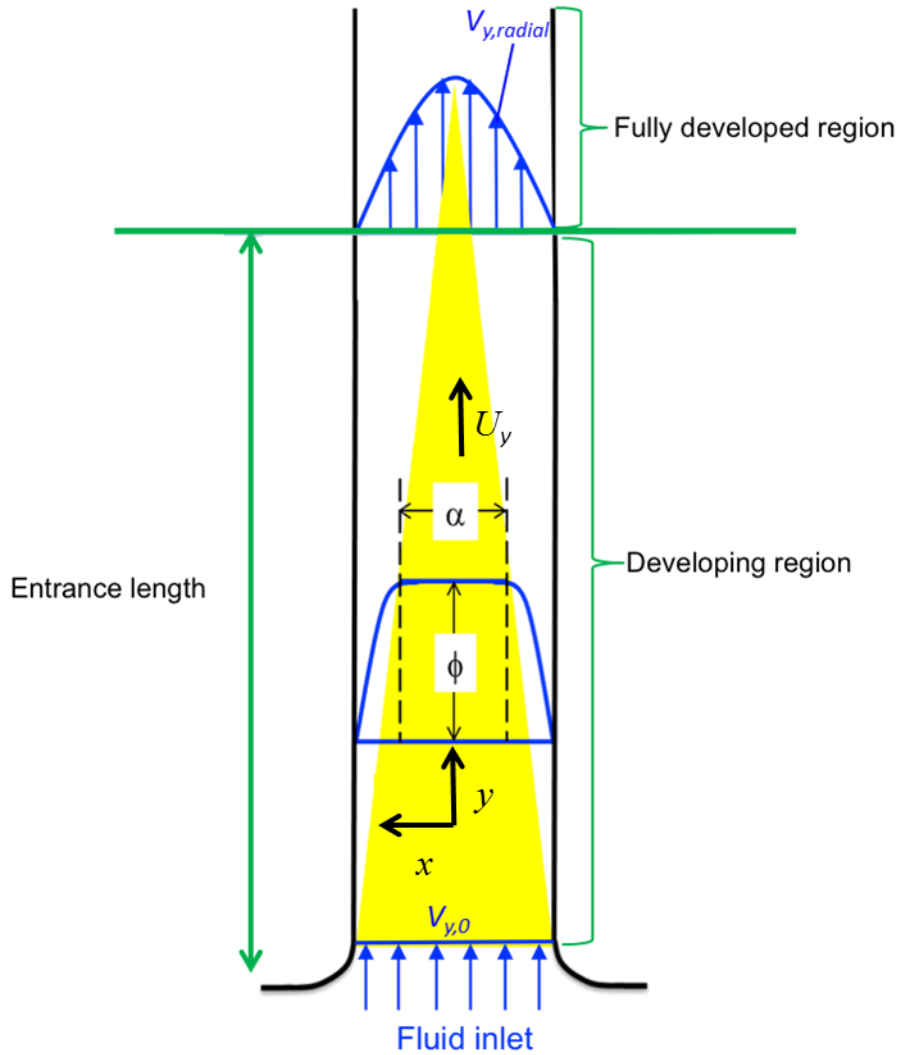


Figure 3: Profile of developing laminar flow velocity (blue lines) and boundary layer expansion (shrinking inviscid core – yellow region).

Two challenges arise in the prediction of particle trajectory within the PIPS tube. First, particle aspiration into the PIPS tube depends on the radial velocity profile that contacts the particle at the tube inlet. Second, even if a particle traverses the inlet, the *developing* flow profile and its corresponding velocity magnitudes within the tube may have an effect on particle collection.

Fargie and Martin (1971) developed an analytical method for determining velocity magnitudes within a tube undergoing laminar boundary layer growth. The method proceeds from boundary layer approximations of continuity and momentum equations, which are summarized below²⁵.

The dimensionless axial velocity (U_y), the dimensionless axial velocity of the inviscid core (ϕ) and the dimensionless radius of the inviscid core (α) are used to describe the axial velocity distribution (Figure 3):

$$U_y = \begin{cases} f & (0 \leq x \leq a) \\ f \left(1 - \frac{x^2 - a^2}{1 - a^2} \right) & (a \leq x \leq 1) \end{cases} \quad (6)$$

where $U_y = V_y/V_{y,0}$, ϕ and α are functions of x only, such that when $x=0$ (tube y -axis of symmetry), $\alpha=\phi=U_y=1$ and x is any radial distance, in the x -direction, between the tube wall and tube radius. Integrating Equation 6 over L_E yields

$$f = \frac{6}{3 + 2a + a^2} \quad (7)$$

For any cross-section (normal to the y -plane) of the tube (Figure 3) the upward air velocity at any radial point ($V_{y,radial}$) is

$$V_{y,radial} = V_0 \times U_y \quad (8)$$

where V_0 is the inlet air velocity. Based on the inverse relationship between ϕ and α , $V_{y,radial}$ decreases from the center of the inviscid core ($V_{y,radial}=2V_0$) to the pipe wall ($V_{y,radial}=0$).

3.1.3. Particle Settling in a PIPS Tube

As noted earlier, the dynamic nature of the fluid profile complicates the prediction of particle trajectory through the tube. To illustrate this, consider a PIPS tube designed to collect particles 50 μm and larger (Figure 4). The inlet air velocity ($V_{y,0}$) is set to $7.0 \text{ cm}\cdot\text{s}^{-1}$. Thus, a settling 50 μm particle of unit density ($V_{ts}=7.83 \text{ cm}\cdot\text{s}^{-1}$) should be aspirated and deposit onto the filter. However, at the top end of the tube, the parabolic profile contributes to differing velocity magnitudes (green and black arrows). At this region of fully developed flow, if a 50 μm particle falls in the path of the

- a) black arrows ($V_{y,radial} < V_{ts}$) then it will traverse through the tube and deposit on the filter.
- b) green arrows ($V_{y,radial} > V_{ts}$), then it will be ejected from the tube. Thus, some particles that should be collected by each tube are actually rejected, resulting in a *rejection error*.

Consider also a 30 μm particle (Figure 4). If this particle falls in the path of the

- 1) black arrows ($V_{y,radial} < V_{ts}$), the particle will be collected. Thus, there is a fraction of particles that should be rejected by each tube that is not collected, resulting in a *collection error*. Collection errors should be negligible, however, because while these particles may be aspirated, they will not reach the filter surface, due to the fact that the filter face velocity ($V_{y,0}$) will be greater than the particle settling velocity ($V_0 > V_{ts}$). The ultimate fate of these particles (i.e., whether they impact on the tube walls or elsewhere) is not considered in the model developed here.
- 2) green arrows ($V_{y,radial} > V_{ts}$) the particle will be rejected outright.

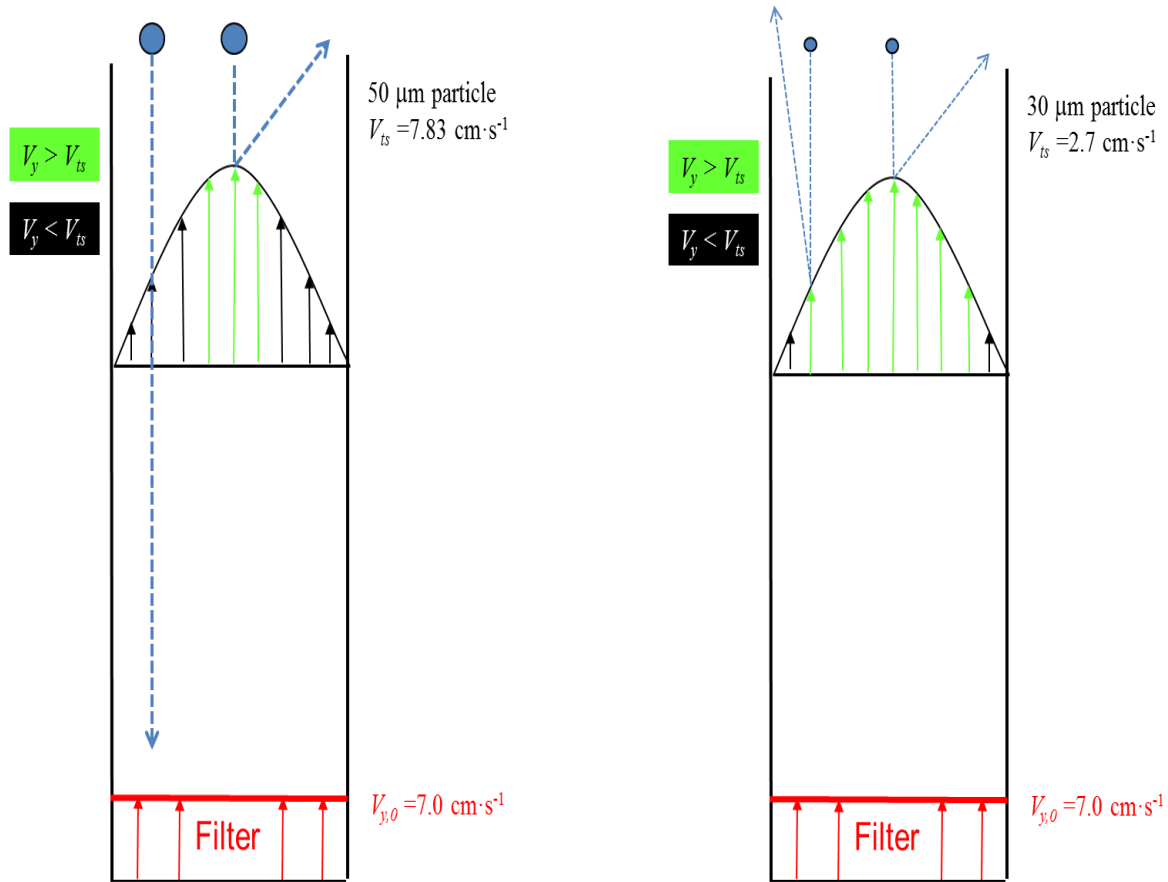


Figure 4: Behavior of 50 μm and 30 μm particles in a PIPS tube

3.1.4. Collection and Rejection Errors Due to Developing Laminar Flow

To determine the fraction of particles that contribute to collection and rejection errors in each tube, the following approach was employed. An inlet air velocity ($V_{y,0}$) was chosen to be slightly less than the terminal settling velocity of the critical (cut-size) particle diameter. Entrance length (L_E) was calculated from tube geometry and flow conditions (Equation 5). The cross sectional area (normal to the y -plane) at the L_E ($\alpha=0$) was divided radially into concentric annuli (Figure 5).

The radius of each circle, x in Equation 6 was used to calculate at the $V_{y,radial}$ for each annulus. The velocities for each concentric circle were compared to settling velocities of

particles from 1-100 μm . For each circle, if $V_{y,radial} < V_{ts}$ then the particle will be collected, and if $V_{y,radial} > V_{ts}$ then the particle will be rejected.

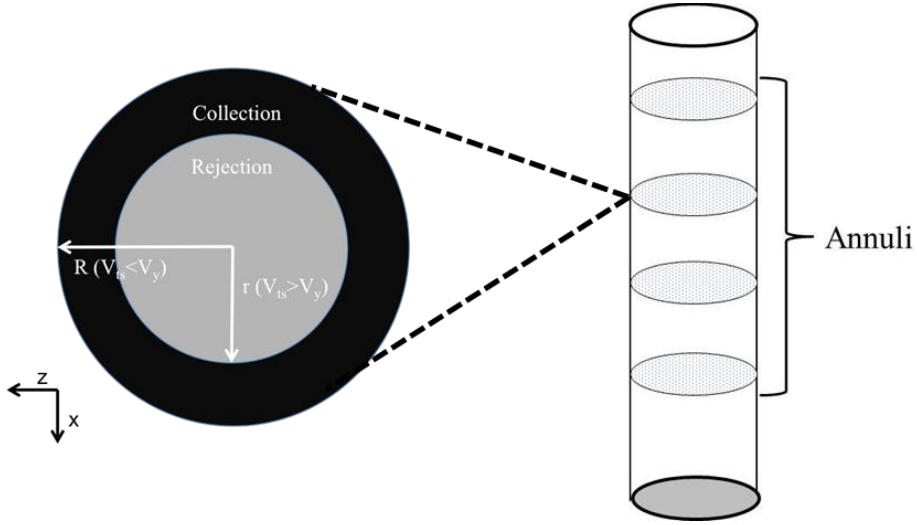


Figure 5: Annular areas of collection and rejection. Each PIPS tube is divided into 100 annuli.

Recall that, velocities are higher closer to the center of the parabolic fluid profile. Thus, particles will experience the highest velocities, closest to the tube center. With the assumptions of a monodisperse particle size distribution at the inlet and a uniform particle concentration, the fraction of particles that will penetrate the tube (sampling efficiency) is the ratio of the collection and rejection annular areas (Figure 5). Thus, the *modeled* sampling efficiency of the tube ($\eta_{mod,i}$) for a given particle size i , or the fraction of particles collected, is

$$\eta_{mod,i} = \frac{Area_{tube} - Area_{rejection}}{Area_{tube}} \quad (9)$$

$$\eta_{\text{mod},i} = \frac{\pi R^2 - \pi r^2}{\pi R^2} \quad (10)$$

$$\eta_{\text{mod},i} = 1 - \left(\frac{r}{R}\right)^2 \quad (11)$$

where R is the tube radius, and r is the radius of the “rejection” annulus. An example plot showing modeled collection efficiency for a tube designed to segregate the aerosol at $50 \mu\text{m}$ is shown in Figure 6. The effects of non-uniform flow yield a modeled collection curve that is less “sharp” than the ideal curve.

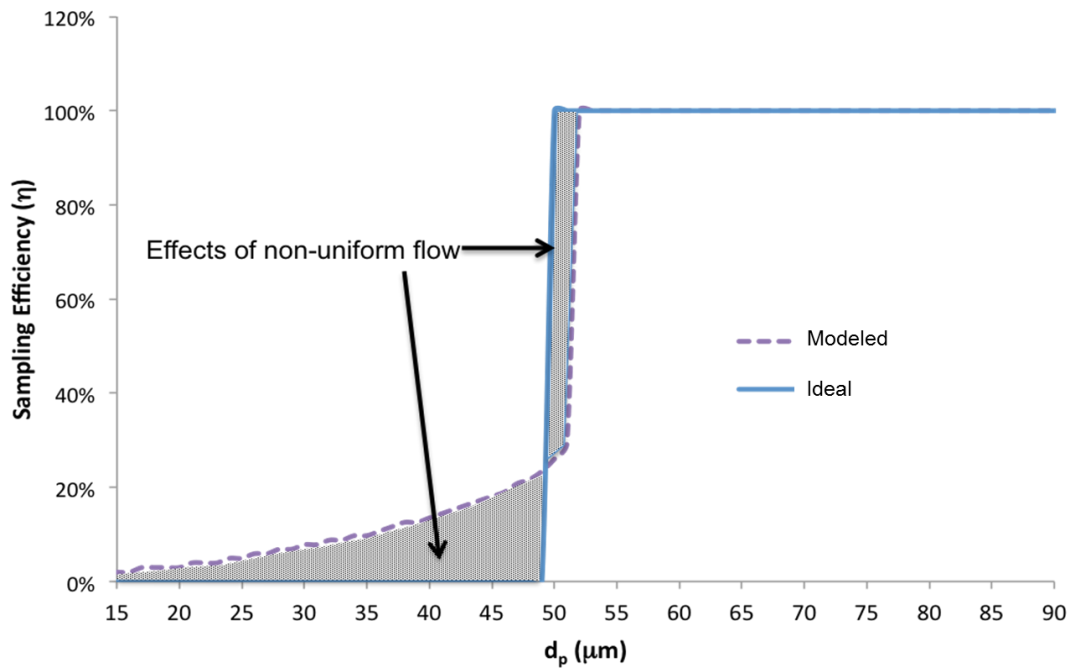


Figure 6: The effects of non-uniform flow for a $50 \mu\text{m}$ cut-size tube.

3.1.5. PIPS Tube Characteristics

To minimize collection and rejection errors, which are proliferated by the non-uniform flow profile, shorter tubes (tube length $< L_E$, $\alpha < 0$) were chosen. As tube length decreases, the effects from non-uniform velocities should decrease, since shorter tubes favor a larger inviscid core and, hence, a more uniform velocity profile throughout the tube cross-section. Ideally, a tube of length 0 m would be least affected by non-uniform flow. However, for practical considerations we chose tube lengths of 1.5 and 5 cm. Tube diameter (ID) was set at 3.2 cm for all tubes, so that each tube could employ a standard 37-mm filter and cassette at the bottom. Selected tube geometries, operation parameters, and modeled cut-sizes and sampling efficiencies are summarized in Table 1.

Table 1: PIPS specifications

Tube Length (cm)	Air Flow Rate (L·min⁻¹)	Cut-size (μm)	$\eta_{mod,i}$ (%)	Percent of L_E (%)
1.5	0.60	20	87	29
	1.35	30	72	13
	2.50	40	20	7
	3.50	50	18	5
5	0.60	20	84	98
	1.35	30	57	44
	2.50	40	13	19
	3.50	50	3	17

3.1.6. Fluid flow assumptions

Two assumptions about the fluid regime outside the PIPS were made. First, that the inlet flow profile through the filter is flat. Second, that the air velocity immediately above the PIPS aspirating head is zero.

3.2. Test chamber

The PIPS was placed inside a vertical test chamber (Figure 7) that dispersed solid aerosol in the form of fluorescent polyethylene spheres (PES). The 2.5 m vertical chamber was constructed to facilitate dispersion and settling of IPM, in the form of PES, in calm air and followed the design of Aitken et al. (1999) and Hsu and Swift (1999)^{23,24}. Aerosol was ejected upward through a HEPA filter and encountered a rotating blade as it settled. Next, the aerosol passed through a honeycomb diffuser to break up any turbulent eddies generated during aerosol generation or mixing. After the diffuser, the well-mixed aerosol settled onto the test section where the PIPS was located.



Figure 7: The 2.5 m laboratory test chamber with aerosol generation and dispersion section (Figure 8) and calm-air test section (Figure 9), and pump.

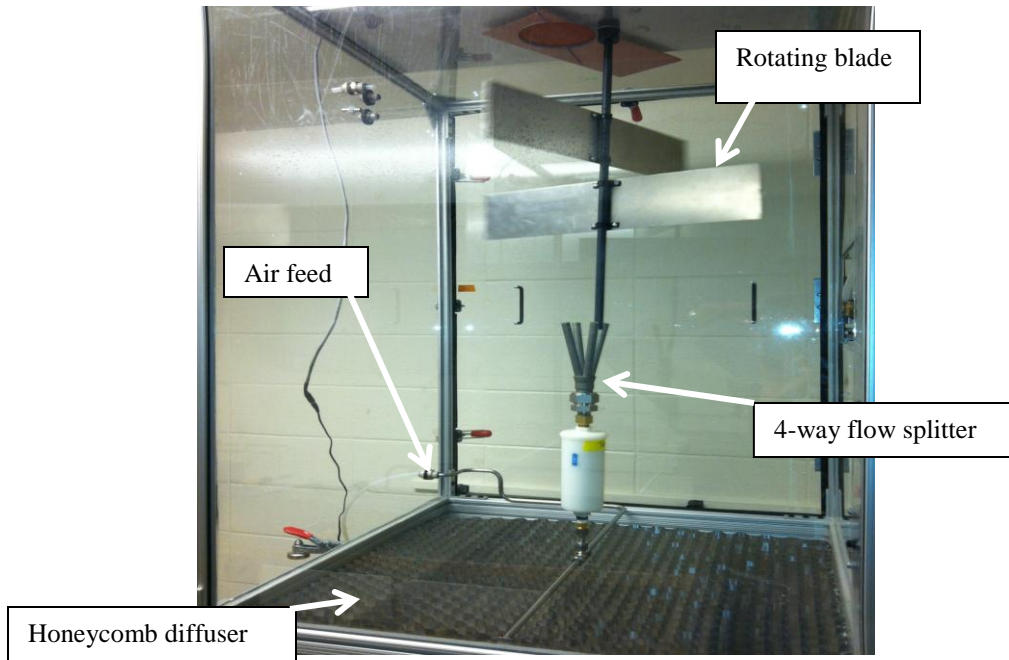


Figure 8: Aerosol generation and dispersion section with rotating blade, dispersion nozzle, air feed and honeycomb diffuser.

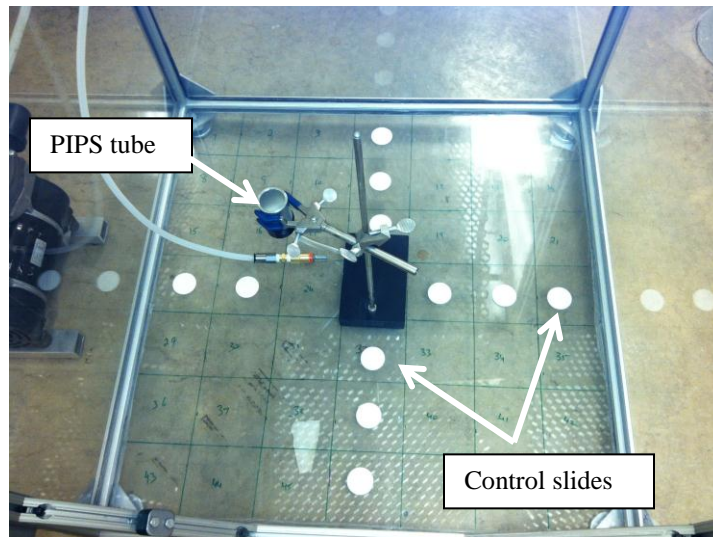


Figure 9: Test section with PIPS tube and control filters.

4. Experimental Method

4.1 Verification of a Calm-air Environment

Velocities were measured using an anemometer (with the rotating blade turned on) in four sections of the test chamber: above the rotating blade, below the rotating blade, above the honeycomb diffuser and at the PIPS height (0.3 m from the chamber floor). Velocities within the range reported by Baldwin and Maynard (1998) for typical workplaces were considered adequate.

4.2 Preparing Aerosol

The test aerosol consisted of fluorescent polydisperse (10-90 μm) polyethylene microspheres (UVYGPMS, Cospheric LLC) of unit density. A fluorescent microscope (Orthoplan, Leica), fluorescent filters (Vivid Plus Set XF05-2/B, Omega Optical) and a micrometer were used to verify size distributions of the test particles. A bolus of these spheres (1.6 g) was inserted into a HEPA filter cassette that served as a suspension medium prior to aerosolization.

4.3 Particle Deposition on the Chamber Floor

To determine whether deposition of particles on the chamber floor was uniform, two experiments were conducted without the PIPS in place. The test aerosol was dispersed and settled onto 25 control filters (Cellulose Support Pad, Pall). From these experiments size

statistics, such as count median diameter (CMD) and geometric standard deviation (GSD) for the test aerosol and spatial variation in chamber deposition were obtained.

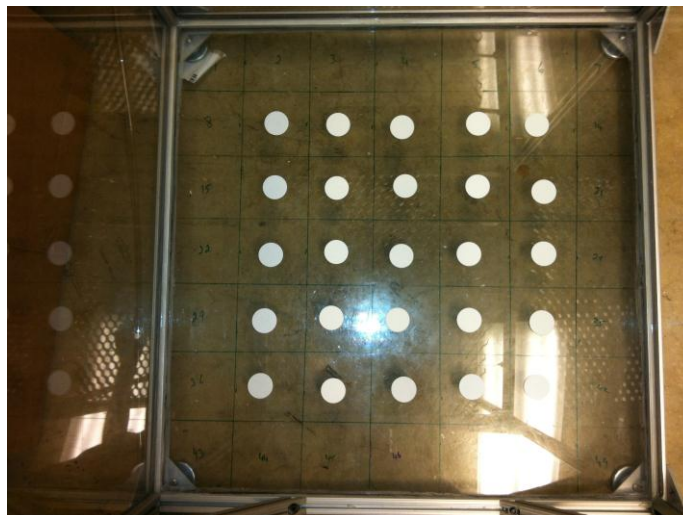


Figure 10: Arrangement of control filters to measure particle deposition on chamber floor.

4.4 Dispersion of polyethylene spheres

The HEPA cassette containing the test aerosol was attached to an aluminum tube that connected to a compressed air source; the other end of the HEPA cassette was attached to a 4-way flow splitter (Figure 8). This step was conducted prior to placing control filters and the PIPS on the chamber floor, ensuring that no contamination of the filters occurred. If the HEPA filter cassette was attached after the control filters and PIPS filter were set, there was a possibility of shaking the assembly and allowing un-mixed particles to fall.

A filter (Cellulose Support Pad, Pall) for the PIPS tube was loaded onto open-faced 37-mm cassette. This type of filter was chosen because of its rigidity under positive pressure compared to conventional filters (e.g. Zeflour, Millipore). The PIPS tube was attached to the cassette and secured tightly.



Figure 11: PIPS tube and 37-mm cassette with filter.

4.5. Regulating PIPS Flow and Placement of Control filters

Once the HEPA filter was in place, a PIPS tube (1.5 cm or 5 cm) was selected and experimental equipment was connected according to Figure 12. A pump (81R, Gast) supplied compressed air that was passed through an air filtration system (Norgen Biotek). A rotameter and an orifice (OKCC) were attached downstream of the filtration system. Prior to placing the PIPS tube in the chamber, a DryCal calibrator (BIOS) was attached to ensure that the air flow through the tube was accurate and steady. The control valve was used to regulate air flow into the orifice. Following flow calibration, the calibrator was removed. The PIPS was placed off-center (Figure 9) because the HEPA filter, situated above center, may contribute to a “dead spot” at the center of the chamber floor.

Control filters (Cellulose Support Pad, Pall) were placed in a grid-pattern on the chamber floor (Figure 10) to measure particle deposition rates across the chamber floor.

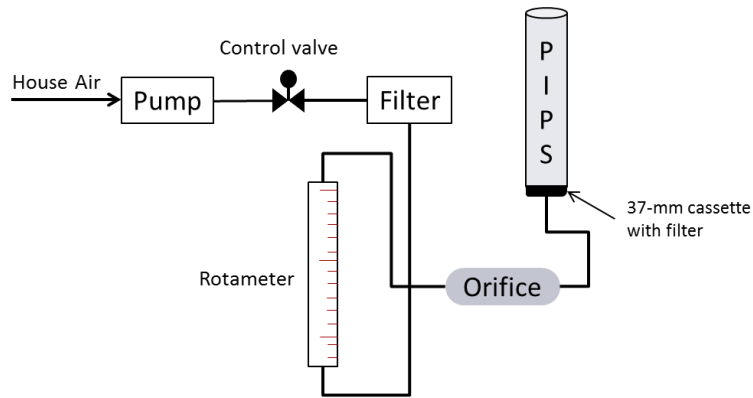


Figure 12: Schematic of PIPS tube and peripherals..

4.6. Aerosol Generation

When the PIPS flow was verified, the door to the test section of the chamber was closed. The motor for the rotating blade was turned on. A solenoid valve was attached to the house air valve. The valve was turned on, and a jet of air passed through the aluminum tube holding the HEPA cassette. Aerosol was ejected upward and was mixed by the rotating blade. The aerosol then settled through the honeycomb diffuser and into the test section. The solenoid valve opened for 5 seconds and closed for 1 minute to allow for proper particle mixing and settling times. The solenoid valve was opened and closed four times for the length of each experiment. The approximate experiment length was 4.5 min.

4.7. Collection of Sampling Media

After the solenoid valve was opened and closed four times, the compressed air valve was closed for the remainder of the experiment. Next, the motor for the rotating blade and pump were turned off. The control filters and the filter from the PIPS (PIPS filter) were labeled and placed in petri dishes for microscopic analysis.

4.8. Experimental Conditions

Two tube lengths and four air flow rates were chosen. Eight experiments were conducted in triplicate for a total of 24 experiments (Table 1). Initially, twelve experiments that included 60 and 70 μm cut-sizes were proposed. However, the corresponding higher flow rates resulted in cracking or buckling of the PIPS filters. Also, high variation in count statistics when air flow rate was increased (to be discussed in later sections) was measured. Therefore, this study was limited to flow rates that allowed the PIPS filter to remain securely in the 37-mm cassette during experiments.

4.9. Measurement of Sampling Efficiency

The measured sampling efficiency of each PIPS tube was determined using epifluorescent microscopy. A fluorescent microscope and ImageJ[®] software were used to measure and compare the distribution of particles on the chamber floor vs. the distribution of particles on the PIPS filter. Since the PIPS is a size-segregating instrument, it is useful to describe the sampling efficiency of each PIPS tube for a user-selected size bin ($\eta_{meas,i}$). The $\eta_{meas,i}$ for each particle size is

$$\eta_{meas,i} = \frac{\bar{N}_{PIPS,i}}{\bar{N}_{control,i}} \quad (12)$$

Where $\bar{N}_{PIPS,i}$ is the average number of particles measured on the PIPS filter for the i^{th} size, and $\bar{N}_{control,i}$ is the average number of particles measured on the control filters for the i^{th} size. The $\eta_{meas,i}$ was compared to design estimations. Coefficients of variation between control filters

($CV_{control}$) were also calculated to quantify variance in particle distribution on the chamber floor. A total coefficient of variation (CV_T) was calculated to take into account variation in chamber deposition and variation in tube sampling efficiency for each experiment. The CV_T was obtained using Equation 13.

$$CV_T = \sqrt{(CV_{filter})^2 + (CV_{controls})^2} \quad (13)$$

Eight independent two-sample t-tests (n=15), using Satterthwaite's approximation for unequal variance, were conducted to evaluate $\eta_{meas,i}$. For each of the eight experimental conditions, two distributions were being compared: the measured and the modeled. With each test, the hypothesis tested was H_0 : There is no difference between the mean measured sampling efficiency ($\bar{\eta}_{meas}$) of the PIPS and modeled mean sampling efficiency ($\bar{\eta}_{mod}$) from design. The experimental conditions from the eight tests are summarized in Table 2

Two-way ANOVA tests were conducted to determine whether tube height, flow rate or an interaction (tube height*flow rate) were factors in $\eta_{meas,i}$. Fifteen tests, one for each size bin shown in Table 2, were conducted.

The results of the ANOVA were used to test two hypotheses: 1) H_0 : There is no difference in $\eta_{meas,i}$ for PIPS tube heights of 1.5 cm and 5 cm. 2) H_0 : There is no difference in $\eta_{o,i}$ for PIPS flow rates of 0.6, 1.35, 2.5 and 3.5 L·min⁻¹.

Table 2: Particle size bins used for two-way ANOVA

Size bins (μm)
10-14
15-19
20-24
25-29
30-34
35-39
40-44
45-49
50-54
55-59
60-64
65-69
70-74
75-79
80-84
85-89
90

All statistical analyses were conducted using SASTM software (version 9.0). Statistical significance was evaluated at the $\alpha=0.05$ level.

4.10. Fluorescent Microscopy

Each filter (PIPS and control) was viewed and imaged using a 1.6x objective lens and a 10x eyepiece. A stage micrometer was used as a reference for ImageJ size analysis. The ImageJ input parameters used to size particles of size $10 < d_p < 90 \mu\text{m}$ are presented in Table 3.

Table 3: User-inputted values for ImageJ

ImageJ Setting	ImageJ Parameter	Value
Scale	Distance in pixels	130
	Known distance (μm)	1000
Particle Analysis	Size (μm^2)	78-6362
	Circularity	0.75-1.00

Microsoft Excel (2011, version 14.1) was used to calculate particle diameters from particle area values reported by ImageJ. Particle count statistics such as sampling efficiencies and coefficients of variation were also generated using Microsoft Excel.

4.11. Tube efficiency

Three additional metrics were chosen to compare the sampling efficiencies from each experimental condition. First, the particle sizes corresponding to 80% ($d_{80\%}$), 50% ($d_{50\%}$) and 20% ($d_{20\%}$) sampling efficiency are identified. Then, a slope based on $d_{80\%}$ and $d_{20\%}$ is calculated. These metrics are convenient because tube efficiency or performance is not solely described by whether a cut-size (i.e., a size corresponding to 50% collection efficiency) was achieved.

5. Results and Discussion

5.1 Size Distribution of Test Aerosol

The polyethylene spheres were of unit density. Therefore, $d_p = d_{ae}$. Size statistics of the test aerosol obtained from experiments without the PIPS in place are summarized in Figures 13 and 14. The distribution is positive-skewed with a geometric standard deviation of approximately 1.7 and count median diameter of approximately 55 μm . The normalized particle counts (Figure 14) show that the aerosol consisted of a greater number of larger particles ($d_p > 55 \mu\text{m}$).

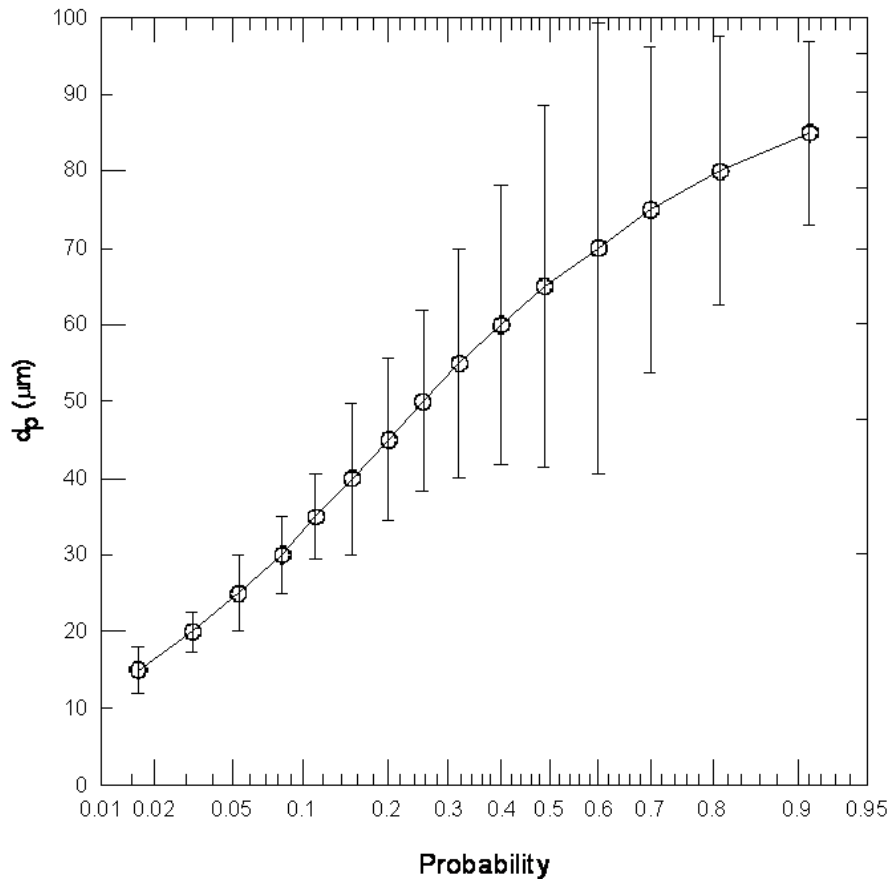


Figure 13: Cumulative particle distribution of test aerosol.

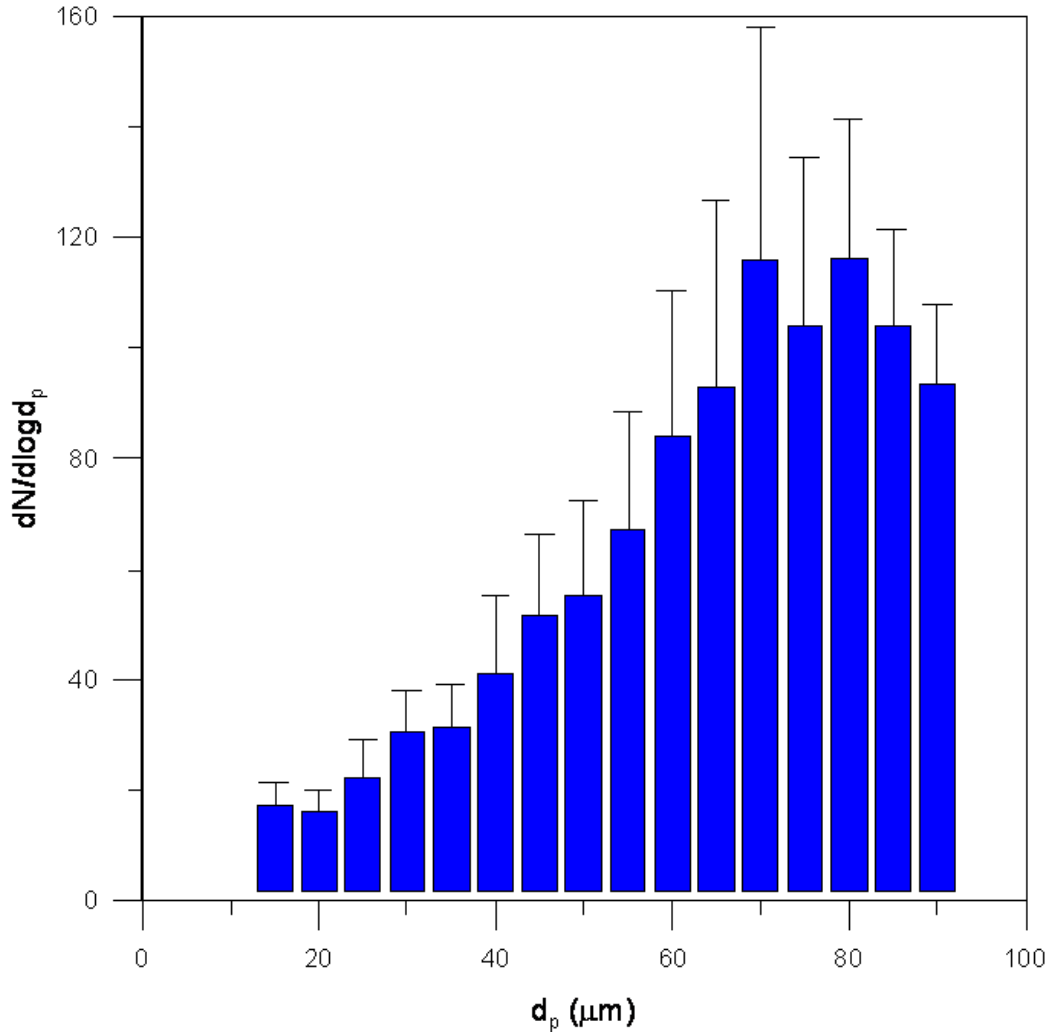


Figure 14: Normalized concentration vs. particle diameter for the test aerosol.

5.2. Mixing of Test Aerosol

Experiments to evaluate the mixing mechanism of the chamber, without the PIPS in place, showed a variation ($CV \approx 30\%$) in particle counts between control filters. Average values for $CV_{control}$ from the eight experiments ranged from 22% to 37%, also indicating that a concentration gradient across the chamber floor was present. The variations may be a result of inadequate mixing by the rotating blade or uneven dispersion of aerosol from the HEPA filter cassette. This variation was taken into account when the total coefficient of variation (CV_T) for the experiment was reported.

The between-filter coefficient of variation was, on average, 30% among all locations. The PIPS was placed in a section of the chamber where the least variation in total particle counts was measured and where counts on adjacent filters varied by no more than 15% (Figure 15).

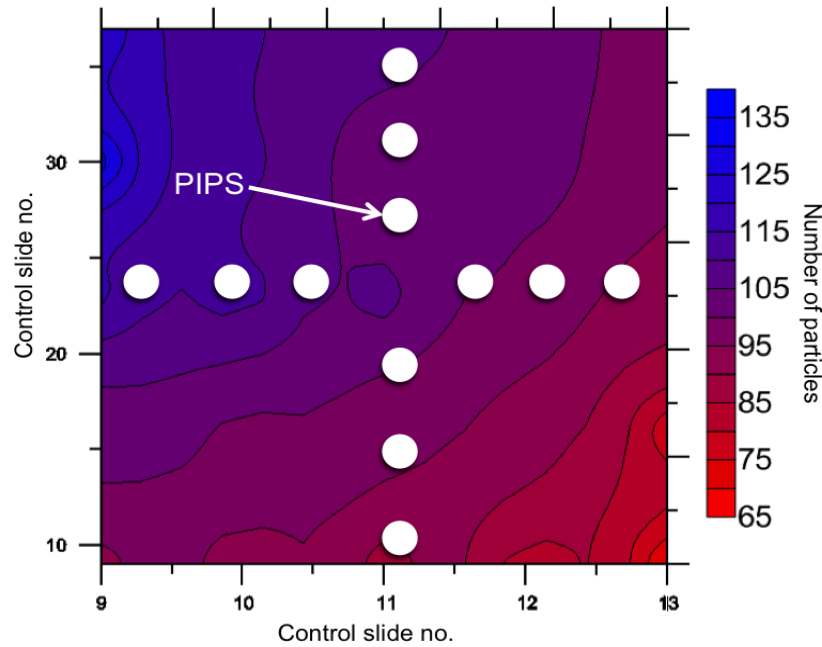


Figure 15: Concentration gradient measured from chamber deposition experiments.

5.3 Calm-air environment

The air velocities from four sections of the test chamber were measured with an anemometer (Alnor AVM440-A) (Table 4). The range of velocities in the chamber (0.05 to 0.10 $\text{m}\cdot\text{s}^{-1}$) was within the range of typical workplaces reported by Baldwin and Maynard (1998).

Table 4: Calm-air measurements of air velocity inside the chamber.

Chamber Area	Average velocity of three measurements ($\text{m}\cdot\text{s}^{-1}$)	Standard Deviation
Above rotating blade	0.05	<0.01
Below rotating blade	0.10	<0.01
Honeycomb diffuser	0.06	0.01
PIPS aspirating head height (4ft. from chamber floor)	0.05	<0.01

5.4. Sampling Efficiency

The results from eight independent two-sample t-tests, which compare mean differences between the measured sampling efficiency, $\bar{\eta}_{meas}$, and the design (modeled) sampling efficiency, $\bar{\eta}_{mod}$, are summarized in Table 5. For each experimental condition, the particle distribution measured on the PIPS filter is compared to the average distribution of the control filters. The hypothesis tested here is H_0 : There is no difference between the mean measured sampling efficiency of the PIPS and modeled mean sampling efficiency.

Table 5: Results from independent two-sample t-tests for differences $\bar{\eta}_{meas}$ and $\bar{\eta}_{mod}$.

Tube Length (cm)	Flow Rate ($L \cdot min^{-1}$)	Cut-size (μm)	$\bar{\eta}_{meas}$	$\bar{\eta}_{mod}$	Pr> t	CV _T (%)
1.5	0.6	20	92	91	0.8939	30
	1.35	30	91	78	0.236	33
	2.5	40	42	64	0.0969	28
	3.5	50	31	57	0.054	33
5	0.6	20	93	92	0.7533	19
	1.35	30	76	82	0.5283	23
	2.5	40	37	67	0.0367	24
	3.5	50	14	55	0.0032	35

The information from Table 5 suggests that the PIPS is – from a statistical standpoint – performing well under most conditions. However, the t-tests alone do not adequately describe sampling efficiency of the instrument. The parameters $d_{20\%}$, $d_{50\%}$ and $d_{80\%}$ are more useful in describing tube performance. The following sections discuss results from each of the experimental conditions.

5.5 PIPS tube for 20 μm cut-size

An average of sampling efficiencies from three experiments for tubes with $Q_0 = 0.6 L \cdot min^{-1}$, $V_0 = 1.32 cm \cdot s^{-1}$ are presented in Figures 16 and 17. For a 20 μm particle, $V_{ts} = 1.33 cm \cdot s^{-1}$.

The sampling efficiencies of both tubes at the cut-size are summarized in Table 7. There was considerable variation in particle deposition on the chamber floor for this experimental condition. The average $CV_{control}$ (variability between filters) was 34% for the 1.5 cm tube and 37% for the 5 cm tube (Figure A1).

The difference between $\bar{\eta}_{mod}$ and $\bar{\eta}_{meas}$ was not statistically significant (1.5 cm: $p=0.8939$, 5 cm: $p=0.7533$), as summarized in Table 7. Sampling efficiencies above 100% were measured for the 1.5 cm tube for $d_p > 60 \mu\text{m}$ and the 5 cm tube for $d_p > 70 \mu\text{m}$. Sampling efficiencies above 100% indicate that the average particle count on the PIPS filter for a given size was greater than the average particle count on the control filters. Standard deviation (SD) error bars are also shown. The total coefficient of variation (CV_T) is calculated using Eq. 13.

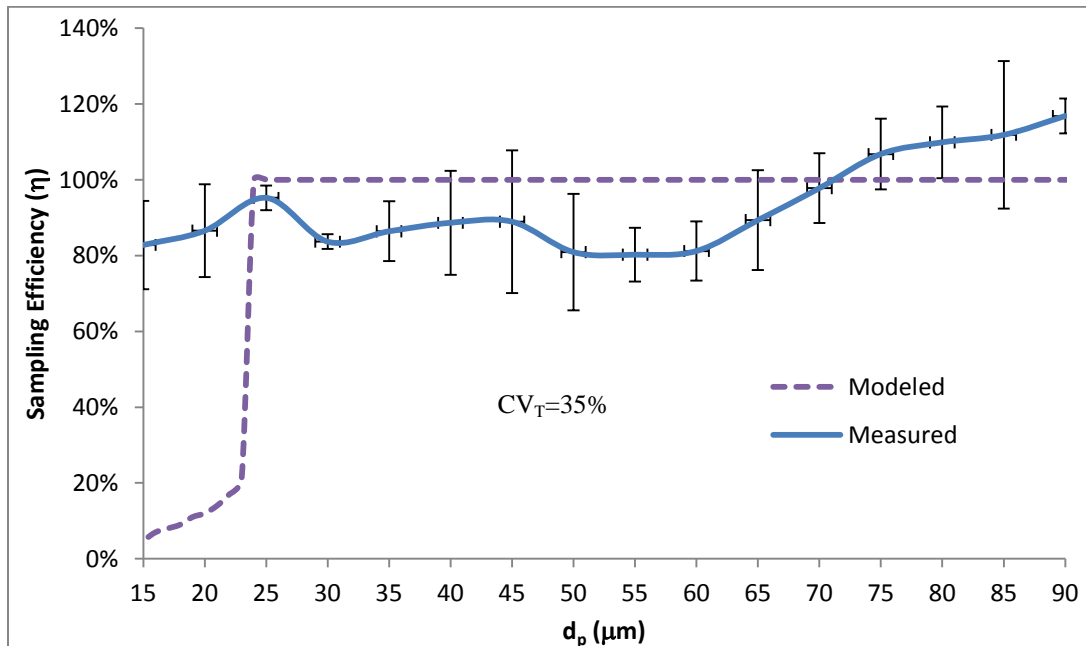


Figure 16: Sampling efficiency for 20 μm cut-size tubes (1.5 cm) with SD error bars.

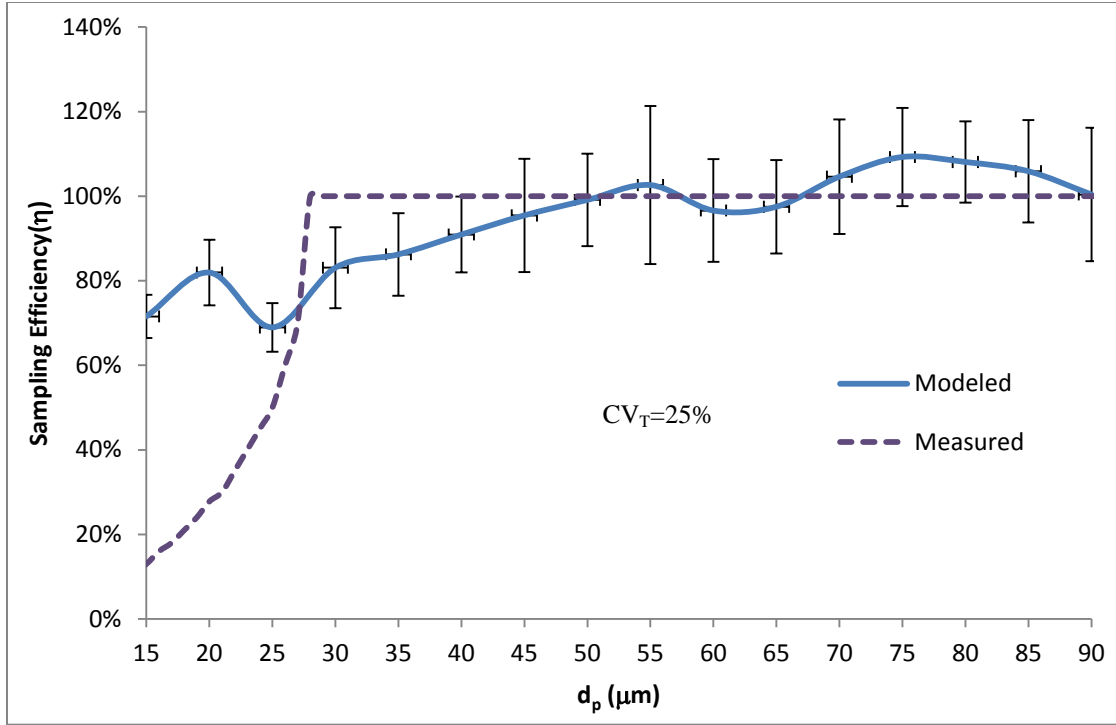


Figure 17: Sampling efficiency for 20 μm cut-size tubes (5 cm) with SD error bars.

5.6 PIPS tube for 30 μm cut-size

An average of sampling efficiencies from three experiments for tubes with $Q_0 = 1.35$ $\text{L}\cdot\text{min}^{-1}$, $V_0 = 3.01$ $\text{cm}\cdot\text{s}^{-1}$ are presented in Figures 18 and 19. For a 30 μm particle, $V_{ts} = 3.01$ $\text{cm}\cdot\text{s}^{-1}$. There was no statistically significant difference between $\bar{\eta}_{mod}$ and $\bar{\eta}_{meas}$ for both tube lengths (1.5 cm: $p = 0.236$, 5 cm: $p = 0.5283$). Lower variation was observed for particle deposition on the chamber floor compared to the 20 μm cut-size experiments (Figure A2).

The average $CV_{control}$ (variability between filters) was 28% for the 1.5 cm tube and 25% for the 5 cm tube. Sampling efficiencies did not follow design estimates for $d_p < 30$ μm . High SDs (up to 50%) were observed for the 1.5 cm tube.

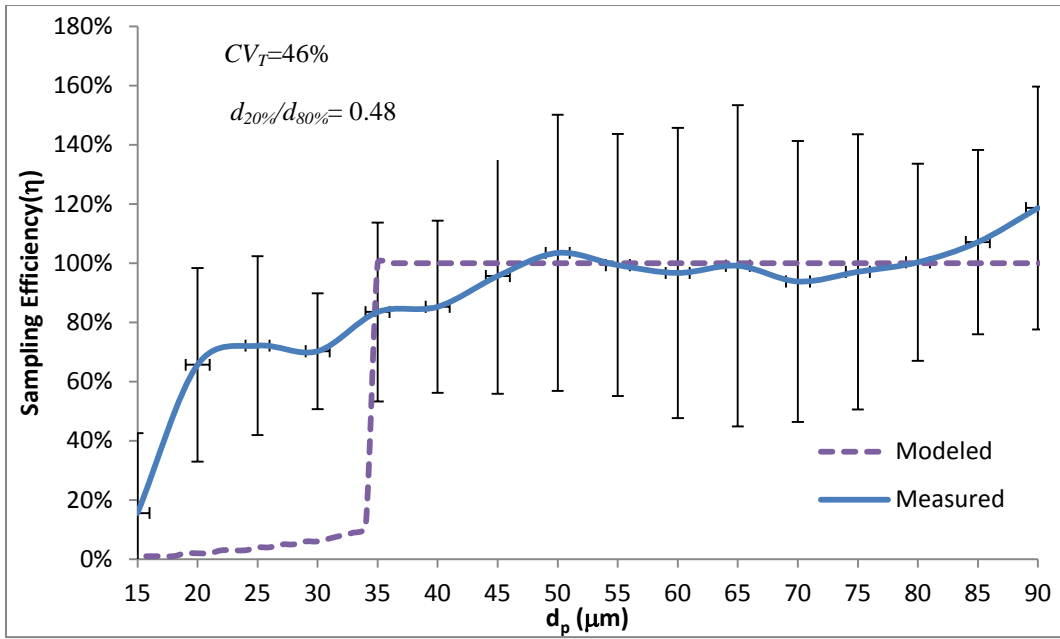


Figure 18: Sampling efficiency for 30 μm cut-size tubes (1.5 cm) with SD error bars.

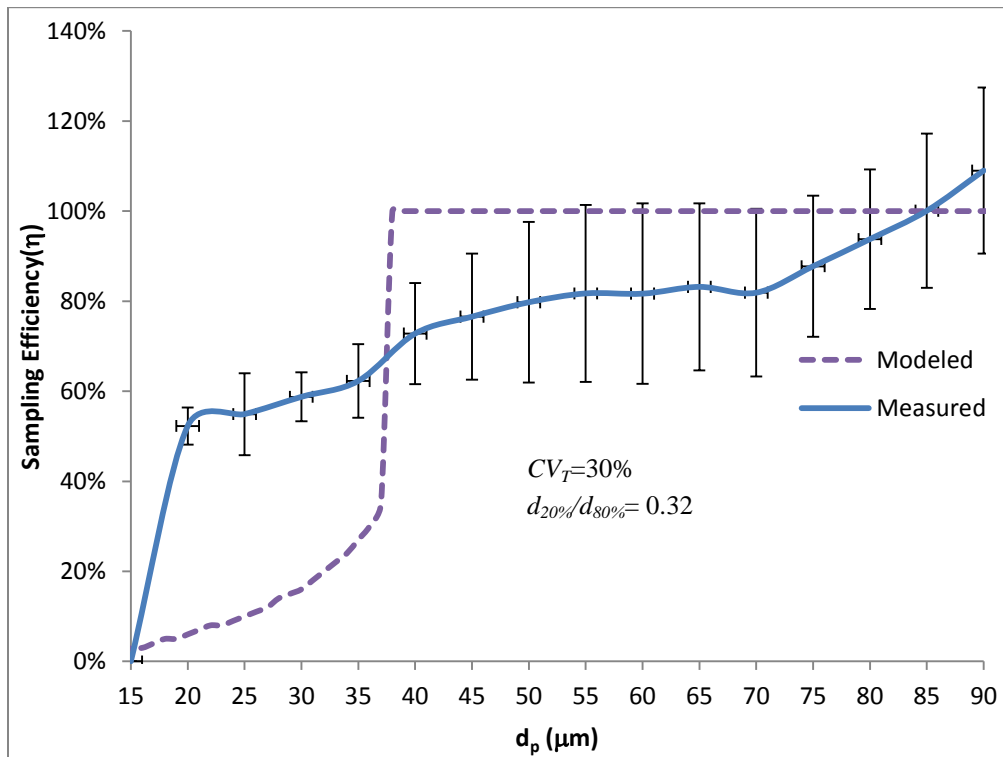


Figure 19: Sampling efficiency for 30 μm cut-size tubes (5 cm) with SD error bars.

5.7 PIPS tube for 40 μm cut-size

An average of sampling efficiencies from three experiments for tubes with $Q_0=2.5$ $\text{L}\cdot\text{min}^{-1}$, $V_0=5.2$ $\text{cm}\cdot\text{s}^{-1}$ are presented in Figures 20 and 21. For a 40 μm particle, $V_{ts}=5.21$ $\text{cm}\cdot\text{s}^{-1}$. There was no statistically significant difference between $\bar{\eta}_{mod}$ and $\bar{\eta}_{meas}$ of the 1.5 cm tube ($p=0.0969$). However, this was not true for the 5 cm tube ($p=0.0367$). Lower variation ($CV_{control}$) was observed for particle deposition on the chamber floor compared to the 20 μm and 30 μm tubes (Figure 24). The average $CV_{control}$ was 26% for both tube sizes (Figure A3). Higher sampling efficiency SDs were observed for both tubes for $d_p>50$ μm .

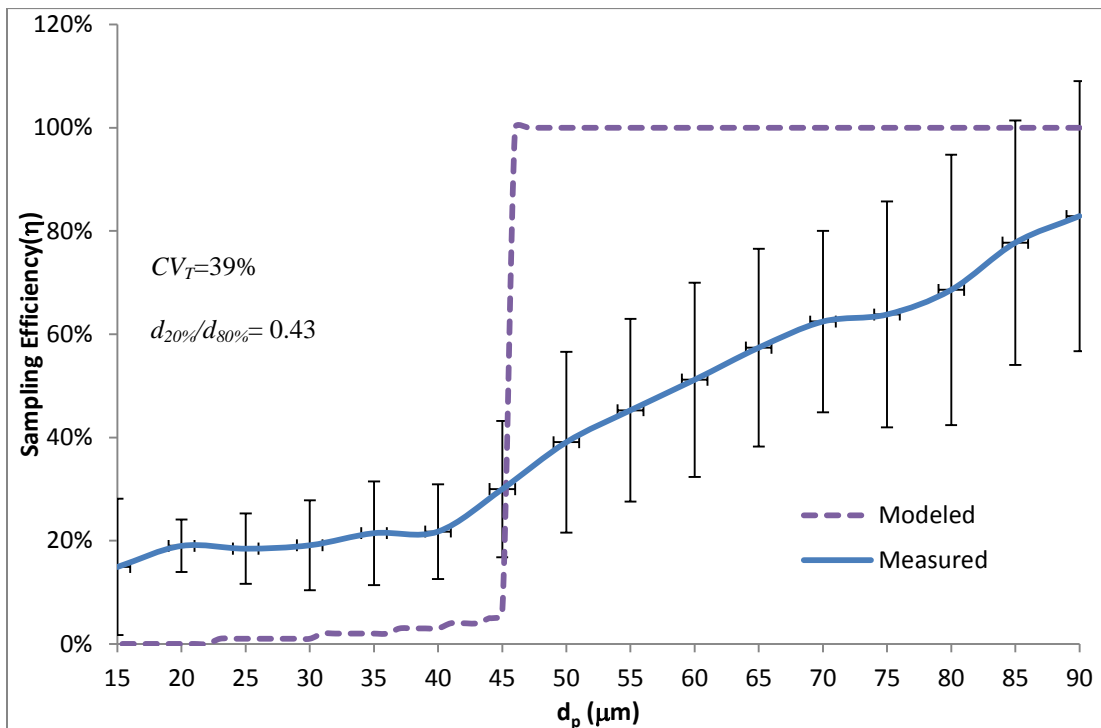


Figure 20: Sampling efficiency for 40 μm cut-size tubes (1.5 cm) with SD error bars.

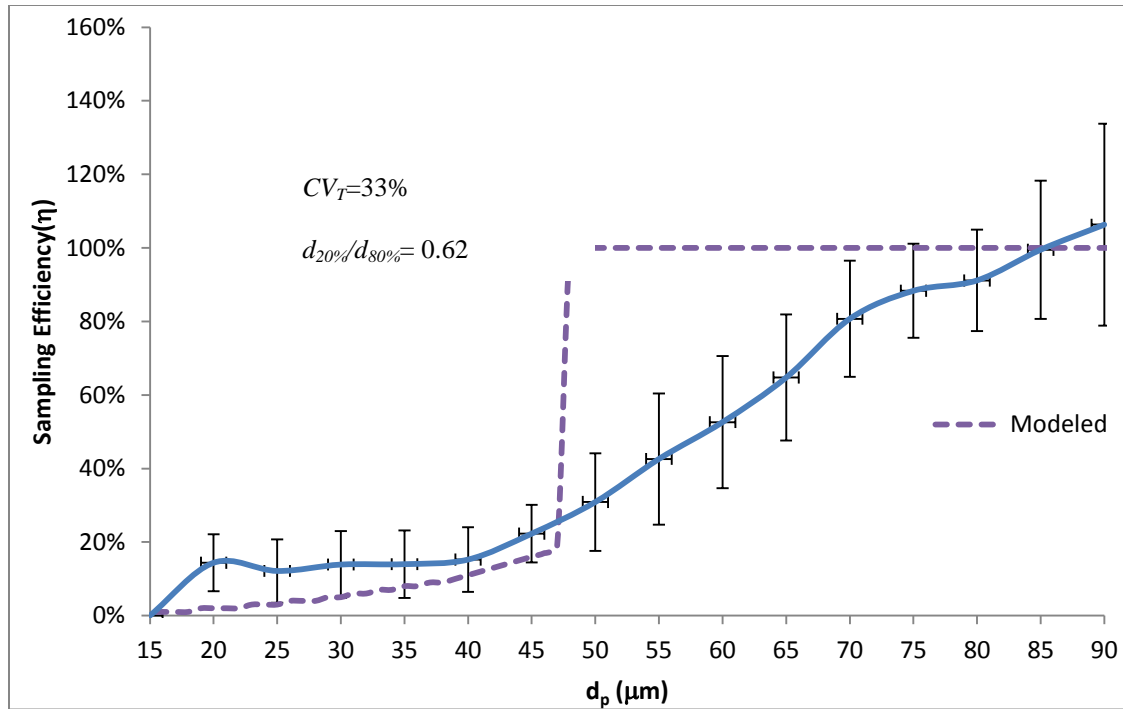


Figure 21: Sampling efficiency for 40 μm cut-size tubes (5 cm) with SD error bars.

5.8 PIPS tube for 50 μm cut-size

An average of sampling efficiencies from three experiments for tubes with $Q_0=3.5$ $\text{L}\cdot\text{min}^{-1}$, $V_0=7.83$ $\text{cm}\cdot\text{s}^{-1}$ are presented in Figures 22 and 23. For a 50 μm particle, $V_{ts}=7.83$ $\text{cm}\cdot\text{s}^{-1}$. The difference between $\bar{\eta}_{mod}$ and $\bar{\eta}_{meas}$ was marginally insignificant ($p=0.054$) for the 1.5cm tube and significant ($p=0.0032$) for the 5 cm tube. Lower variation ($CV_{control}$) was observed in particle deposition on the chamber floor compared to the 20 μm and 30 μm tubes (Figure A4). The average $CV_{control}$ was 30% for the 1.5 cm tube and 22% for the 5 cm tube.

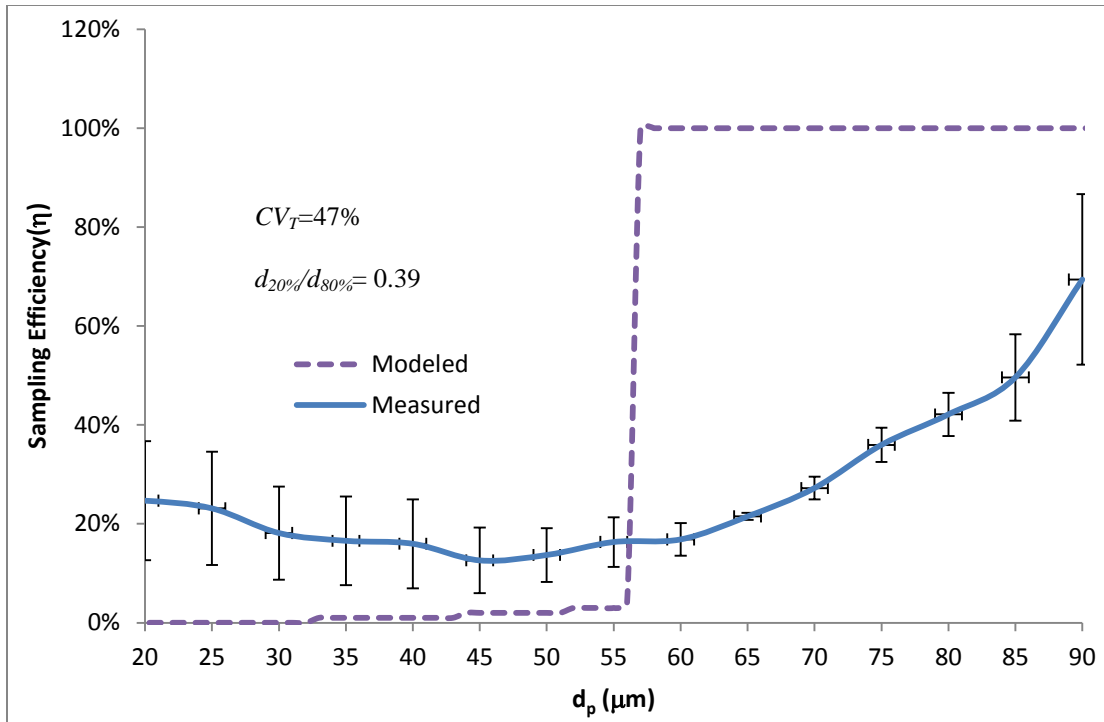


Figure 22: Sampling efficiency for 50 μm cut-size tubes (1.5 cm) with SD error bars.

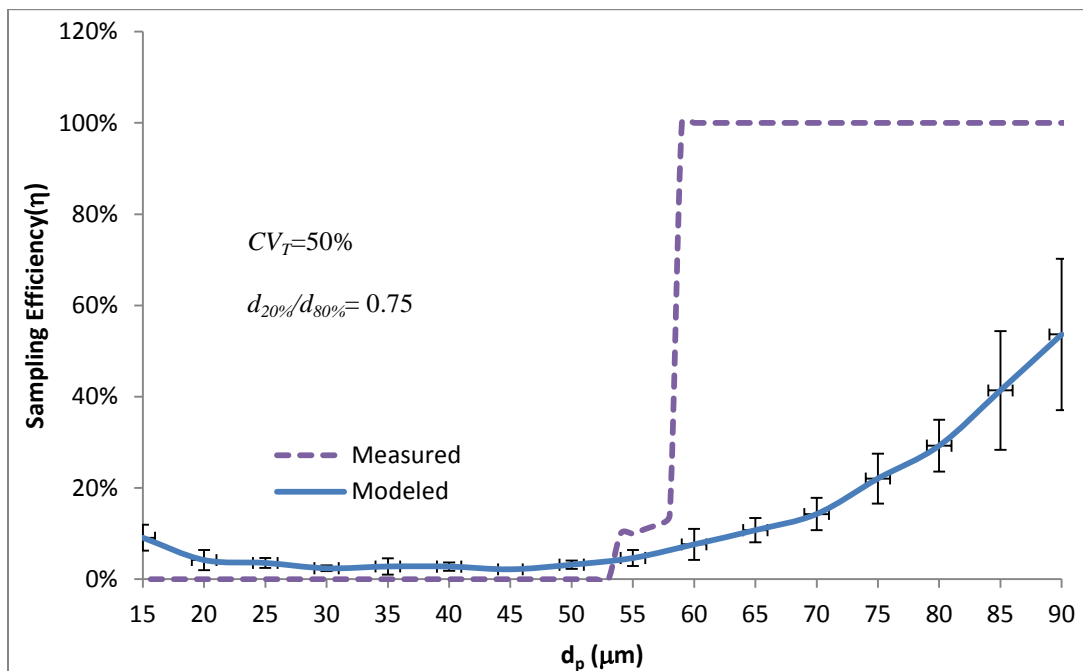


Figure 23: Sampling efficiency for 50 μm cut-size tubes (5 cm) with SD error bars.

5.9 Sampling efficiencies for particle size bins

Two-way ANOVA tests were conducted to determine whether tube height, flow rate or an interaction of both were factors in sampling efficiencies for each size bin. All tests showed that flow rate was a factor in sampling efficiency for all size bins. Tube height was not a factor for particles with $d_p > 60 \mu\text{m}$.

The two-way tests also included an interaction (tube height*flow rate). When the interaction was found to be insignificant, it was removed from the model. Table 6 summarizes the results from the regression models. The interaction between flow rate and tube height was not significant for particles with $d_p > 70 \mu\text{m}$ and for the $d_p > 40 \mu\text{m}$ size bin.

Table 6: Results from two-way ANOVA tests of flow rate, tube height and their interaction (flow rate*tube height).

Size bin (μm)	Flow rate (Pr>F)	Tube Height (Pr>F)	Flow rate*Tube Height (Pr>F)
20>	<.0001	0.0057	0.0169
25>	<.0001	0.0006	0.0213
30>	<.0001	0.0006	0.0137
35>	<.0001	0.0005	0.0109
40>	<.0001	0.01	0.0505
45>	<.0001	0.01	0.0242
50>	<.0001	0.0058	0.0085
55>	<.0001	0.0046	0.0038
60>	<.0001	0.0448	0.0181
65>	<.0001	0.1146	0.0387
70>	<.0001	0.1175	>0.05
75>	<.0001	0.2342	>0.05
80>	<.0001	0.342	>0.05
85>	0.0017	0.6612	>0.05
90>	0.0008	0.5788	>0.05

5.10 PIPS velocity and chamber deposition

Although it was confirmed that the chamber contained a calm-air environment, the results thus far have shown that there was a difference in particle deposition onto the control filters when the PIPS was operating. This section compares the collection efficiency of the PIPS when not operating (no airflow) with conditions previously reported in Sections 5.4 to 5.8. The three operating conditions are: no flow (PIPS off), low flow (0.6 Lmin^{-1} , $20 \mu\text{m}$ cut-size) and high flow (3.5 Lmin^{-1} , $50 \mu\text{m}$ cut-size).

Two flow conditions are presented in Figure 24 for a control filter that is situated close to the PIPS tube. When contrasting the two conditions, there is change in size distribution at $70 \mu\text{m}$ due to the operating PIPS. Results from other control filters close to the PIPS tube show similar trends and are reported in the Appendix as Figures A5-6.

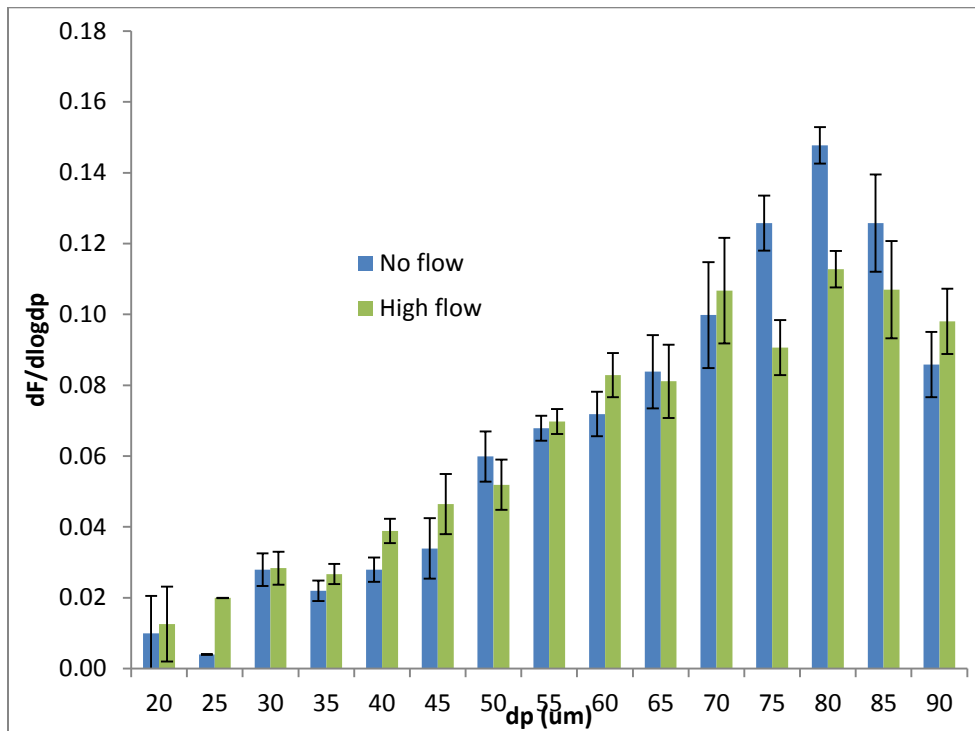


Figure 24: Change in size distribution due to the operating PIPS for control filter 1.

Two sets of control filters, one set closest to the PIPS (Control Filters 1, 4 and 7) and one set farthest from the PIPS (Control Filters 3, 6 and 9), were chosen to assess whether the airflow from the PIPS was causing a change in particle deposition on the control filters. The “PIPS effect” identified by calculating the fractional difference between the “PIPS off” and “PIPS flow” conditions. The differences are first quantified by calculating $dF/d\log d_p$ for each size bin for “PIPS off” and “PIPS on” conditions. Next, $dF/d\log d_p$ for each size bin for “PIPS on” condition is subtracted from the “PIPS off” condition resulting in a fractional difference for each size bin (σ).

$$\sigma_{ith\ size\ bin} = \left(\frac{dF}{d\log d_p}_{ith\ size\ bin, PIPS\ on} \right) - \left(\frac{dF}{d\log d_p}_{ith\ size\ bin, PIPS\ off} \right) \quad (14)$$

Figures 26-28 show the effect of the PIPS resulting from high flow. If there was no PIPS effect on the control filters, then data points in the three figures would each be zero or close to zero; this not the case. Interestingly, the particle distribution changes for some segments of the curve. The PIPS seems to have a different effect for small ($d_p < 50\ \mu\text{m}$), mid-sized ($50 < d_p < 65\ \mu\text{m}$) and large particles ($d_p > 65\ \mu\text{m}$).

The error bars in Figures 26-28 are calculated using the propagation of errors technique for standard deviations. The total error for the high flow condition for each size bin is

$$SD_{total} = \sqrt{(SD_{high\ flow})^2 + (SD_{no\ flow})^2} \quad (15)$$

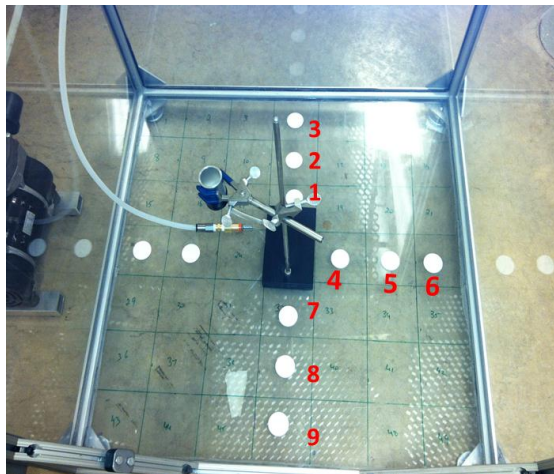


Figure 25: Control filters used to measure PIPS effect.

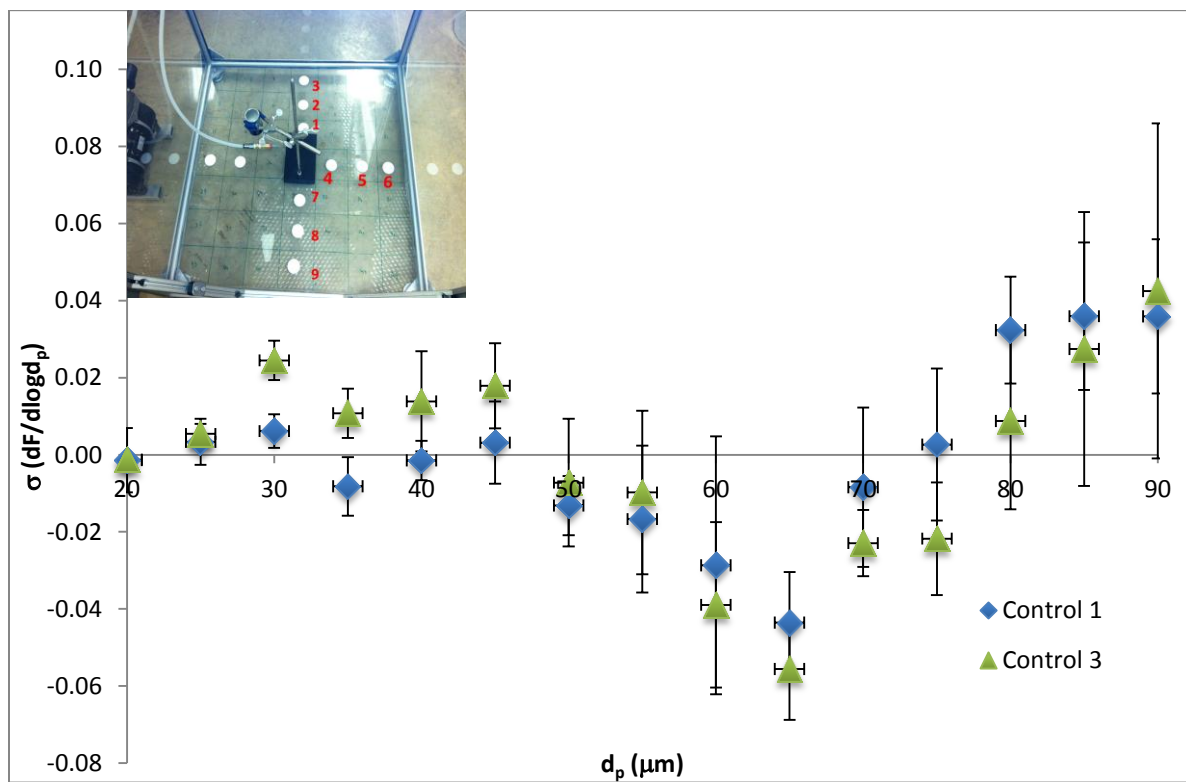


Figure 26: The effect of the high flow PIPS condition on control filter particle deposition.

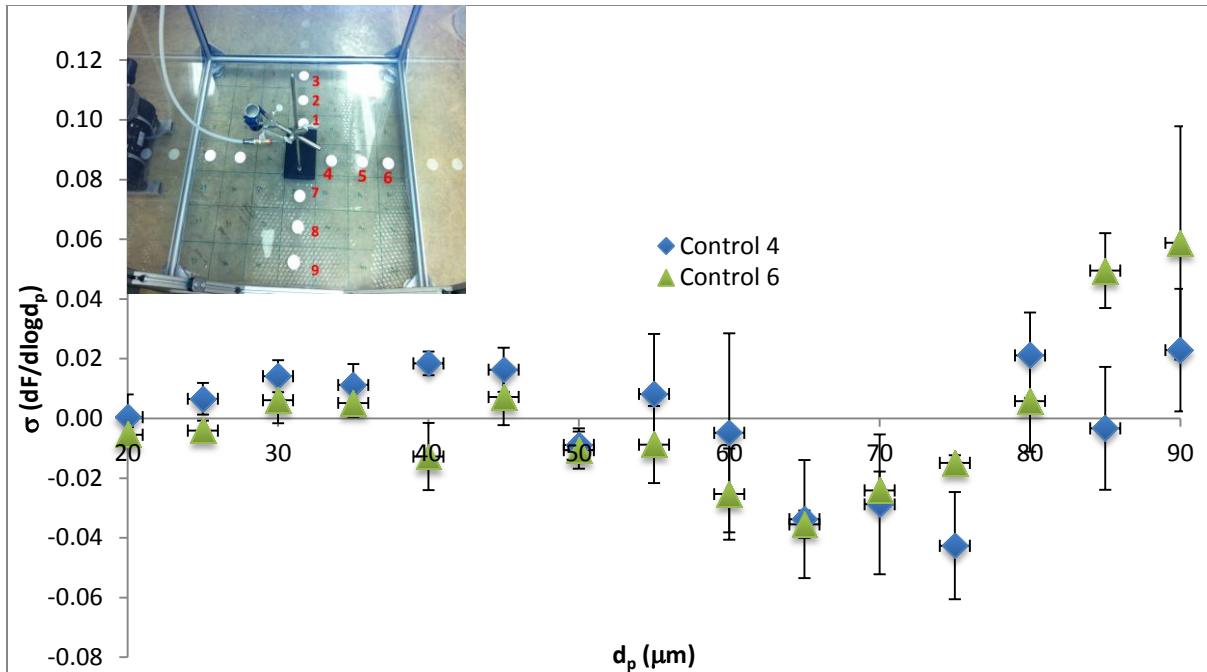


Figure 27: The effect of the high flow PIPS condition on control filter particle deposition.

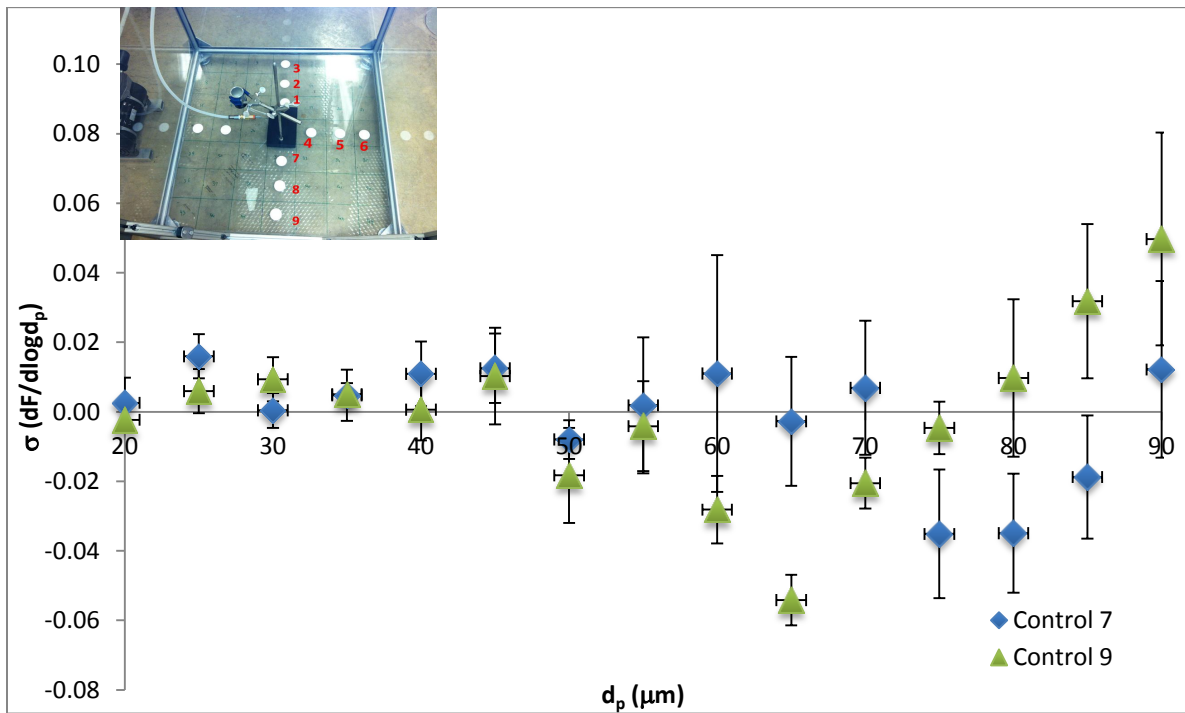


Figure 28: The effect of the high flow PIPS condition on control filter particle deposition.

Similar figures for the low flow conditions are presented in the Appendix as Figures A7-A12. They are not shown here because similar conclusions can be drawn from that PIPS condition as well.

5.11 Fluid flow assumptions

Two assumptions regarding fluid flow were adopted in the PIPS design as previously described in Sec. 5.1.6. To evaluate these assumptions, a model, based on fully developed flow, for each PIPS experimental condition was developed. These models assume that the flow profile at the filter is parabolic – not flat. In Figure 29, the PIPS model that is based on the flow profile for a 5 cm tube at 2.5 Lmin^{-1} ($40 \mu\text{m}$ cut-size) is compared to a model based on fully developed flow. Additional comparisons are presented in Figures A13-A19.

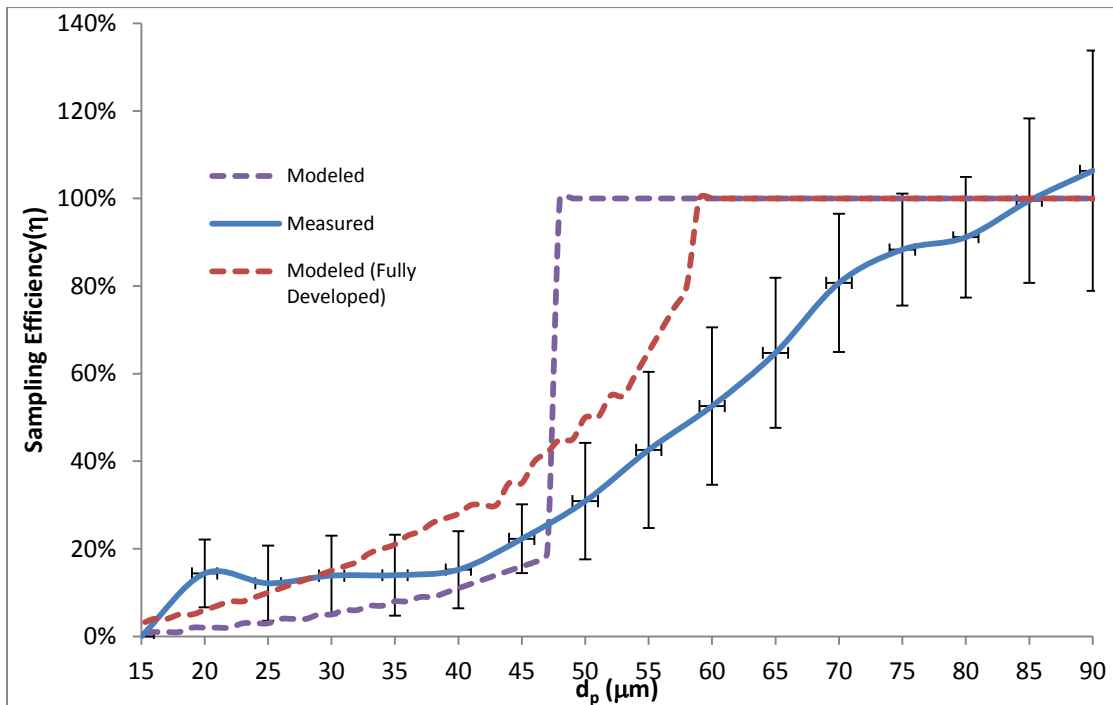


Figure 29: Sampling efficiency of 40um cut-size tubes (5 cm) compared to developing and fully-developed flow.

6. Conclusions and Suggested Future Work

There were two aims of this study: 1) to design and test a two-stage vertical test chamber that would provide a means to study inhalable dust under a calm-air environment 2) to design and test a Portable Inhalable Particle Spectrometer (PIPS) that will report inhalable dust size distributions in calm-air environments. Such an instrument would aid the industrial hygienist in accurately reporting size distributions for the determination of exposure assessment and design of controls.

Velocity measurements verified the presence of a calm-air environment inside the test chamber. The range of velocities in the chamber (0.05 to $0.10 \text{ m}\cdot\text{s}^{-1}$) was within the range of typical workplaces as reported by Baldwin and Maynard (1998)²⁰.

Independent two-sample t-tests that compared measured mean sampling efficiencies and modeled mean sampling efficiencies showed that the $20 \text{ }\mu\text{m}$ cut-size tubes performed closest to design estimations. As tube cut-size increased (along with flow rate), the difference between $\bar{\eta}_{mod}$ and $\bar{\eta}_{meas}$ became more statistically significant.

Two-way ANOVA tests were conducted to determine whether tube height, air flow rate or and interaction (tube height*flowrate) were factors in measured sampling efficiencies for each size bin ($\eta_{meas,i}$). Tube height was a statistically significant factor for all size bins. For particles with $d_p > 65 \text{ }\mu\text{m}$, tube height was a factor. The interaction was a factor for particles with $d_p > 70 \text{ }\mu\text{m}$ and marginally significant for the $d_p > 40 \text{ }\mu\text{m}$ size bin only.

The PIPS prototype has been shown to reject particles, but not as efficiently as designed. Potential contributors to this inefficiency are the effects of the operating PIPS and the chamber design. Four areas warrant further study:

1. *Aspirating head:* The fluid regime at the aspirating head of the PIPS tube warrants further study. The presence of a dissipating jet, emanating from the PIPS, may be interfering with particle collection. This “PIPS effect”, which was demonstrated at several locations in the chamber, appears to bias the same control filters that are used to assess PIPS efficiency. From the experiments conducted, the PIPS effect is also size dependent and spatially not uniform; smaller particles experience a different effect than mid-sized and larger particles. The PIPS effect has on control filter deposition can be better investigated via computational fluid dynamics (CFD) models and additional experiments.
2. *Aerosol dispersion:* The dispersion of particles from the HEPA filter may not be uniform. A more improved dispersion mechanism that allows the user to confidently determine the quantity of particles emitted would be of benefit.
3. *Mixing mechanism:* The rotating speed and blade length of the mixing mechanism may not be achieving a homogenous environment. A CFD model would also help in designing a better mixing apparatus.
4. *Control filters:* The distance between control filters, the number of control filters and the size of control filters should be evaluated. The size and type of control filters used in this study were chosen to match the filter used by the PIPS. Using a different type of filter or less filters of a larger size may add to a better

understanding of the areas mentioned above. One advantage of using a smaller number control filters is that less time is spent imaging and counting particles.

After addressing these four areas, the PIPS can be evaluated using multiple tubes simultaneously in a workplace environment.

7. References

1. NIOSH, *Work-Related Lung Disease Surveillance System (eWoRLD)*. U.S. Department of Health and Human Services, Public Health Service, Centers for Disease Control and Prevention, National Institute for Occupational Safety and Health, Division of Respiratory Disease Studies, Surveillance Branch. Available at:
<<http://www2a.cdc.gov/drds/WorldReportData/>> [Accessed May 25 2011].
2. Spaan, S., et al., *Exposure to inhalable dust and endotoxins in agricultural industries*. Journal of Environmental Monitoring, 2006. **8**(1), 62-72
3. Omland, O., *Exposure and respiratory health in farming in temperate zones – a review of the literature*. Ann Agric Environ Med, 2002. **9**(2), 119-136
4. Hendrick, D.J., *Occupation and chronic obstructive pulmonary disease (COPD)*. Thorax, 1996. **51**(9), 947-955.
5. Beckett, William S., *Occupational Respiratory Diseases*. New England Journal of Medicine, 2000. **342** (6), 406-413.
6. Greaves, I.A., et al., *Respiratory health of automobile workers exposed to metal-working fluid aerosols: respiratory symptoms*. American Journal of Industrial Medicine, 1997. **32**(5), 450-459.
7. Musk, A.W., et al., *Respiratory symptoms, lung function, and sensitisation to flour in a British bakery*. British Journal of Industrial Medicine, 1989. **46**(9), 636-642

8. Cooper, M.R., Susi, P. & David. R, *Evaluation and control of respirable silica exposure during lateral drilling of concrete*. Journal of Occupational and Environmental Hygiene, 2012. **9**(2): p D35-D41.
9. IARC/WHO, *IARC Monographs on the Evaluation of Carcinogenic Risks to Humans, 62: Wood Dust and Formaldehyde*. IARC, 1995.
10. Spear, T.M et al., *Assessment of particle size distributions of health-relevant aerosol exposures of primary lead smelter workers*. Ann. Occup. Hyg., 1998. **42**(2): p 73-80.
11. NIOSH, *Aerosol Program Assessment Committee Report*. 2003, CDC.
12. Vincent, J.H., *Particle Size-Selective Sampling for Particulate Air Contaminants*. 1999, Cincinnati, Ohio: ACGIH.
13. Hinds, W.S., *Aerosol Technology*. John Wiley & Sons, Inc., 1999. pp. 2-12, 111-152.
14. ACGIH, *2011 Threshold Limit Values and Biological Exposure Indices*. 2011, American Conference of Governmental and Industrial Hygienists, Cincinnati, OH.
15. Paik, S.Y. and Vincent, J.H., *The orientation-averaged aspiration efficiency of IOM-like personal samplers mounted on bluff bodies*. Ann. Occup. Hyg., 2004. **48**(1): pp. 3-11.
16. Kenny, L.C., et al., *The sampling efficiency of personal inhalable aerosol samplers in low air movement environments*. J. Aerosol Sci., 1999. **30**(5): p 627-638.
17. Koehler, K.A., et al., *Solid versus Liquid Particle Sampling Efficiency of Three Personal Aerosol Samplers when Facing the Wind*, Ann. Occup. Hyg., 2012. **56**(4): pp. 194-206.
18. Mark, D. and Vincent, J.H., *A New Personal Sampler for Airborne Total Dust in Workplaces*, Ann. Occup. Hyg., 1986. **30**(1): pp. 89-102.

19. Harper, M. and Lidén, Göran, *The Need for an International Sampling Convention for Inhalable Dust in Calm Air*. Journal of Occupational and Environmental Hygiene, 2006. **3**(10): D94-D101.
20. Baldwin, P.E. & Maynard, A.D., *A Survey of Wind Speeds in Indoor Workplaces*. Ann. Occup Hyg., 1998. **42**(5): p 303-313.
21. Sleeth, D.A and Vincent, J.H., *Inhalability for aerosols at ultra-low windspeeds*. J. Phys.: Conf. Ser. **151** (2009) 012062
22. Schmees, D.K , et al., *Experimental methods to determine inhalability and personal sampler performance for aerosols in ultra-low windspeed environments*. J. Environ. Monit., 2008. **10**(12): pp. 1426-36.
23. Aitken, R.J. et al., *Aerosol inhalability in low air movement environments*. J. Aerosol Sci., 1999. **30**(5): p 613-626.
24. Hsu, D and Swift, D.L., *The measurement of human inhalability of ultralarge aerosols in calm air using mannikins*. J. Aerosol Sci., 1999. **30**(10), 1331-1343. Fargie, D. and Martin, B.W., *Developing laminar flow in a pipe of circular cross section*. Proc. R. Soc. Lond. A., 1971. **321**(1547) 461-476.

APPENDIX

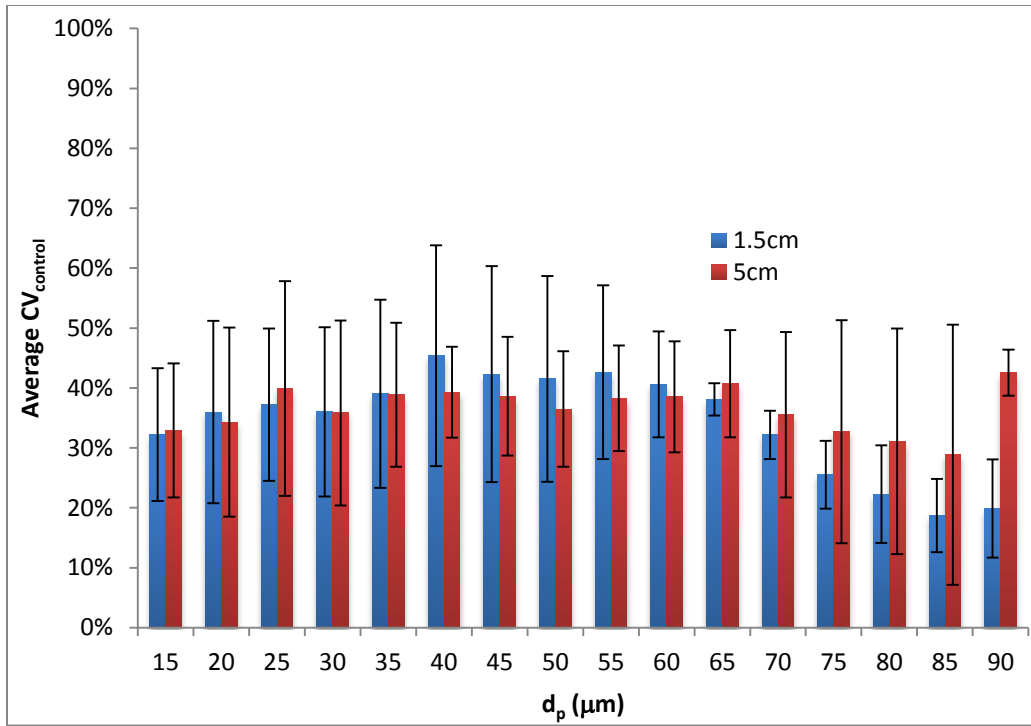


Figure A1: Average $CV_{control}$ per size bin, for 20 μm cut-size tubes.

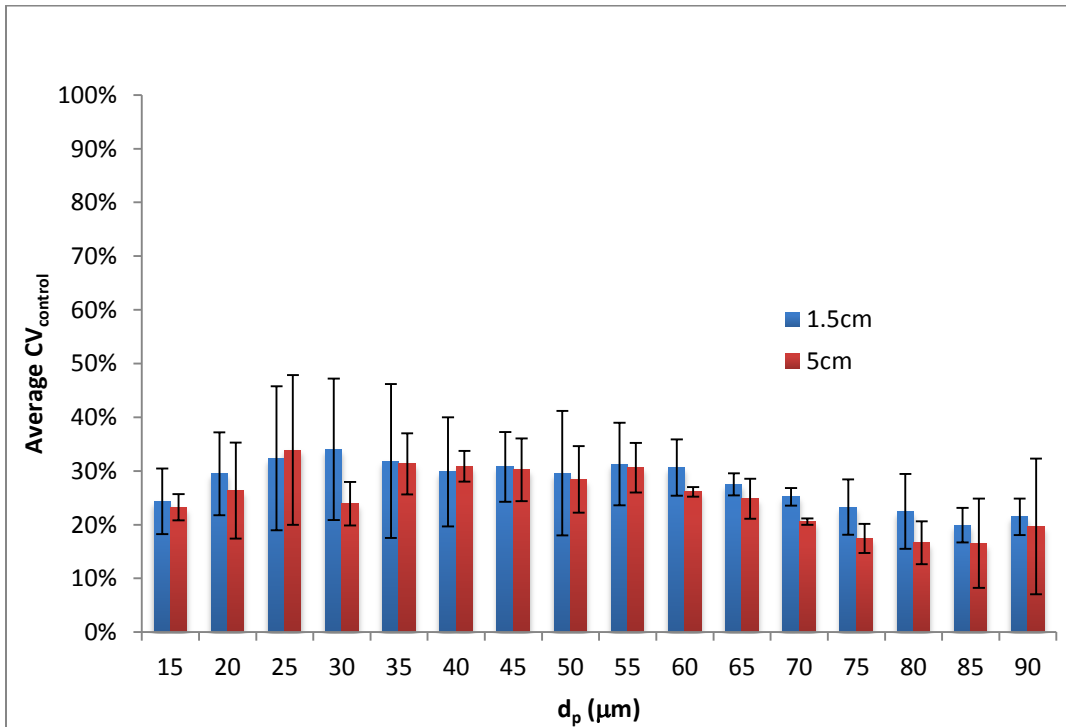


Figure A2: Average $CV_{control}$ per size bin, for 30 μm cut-size tubes.

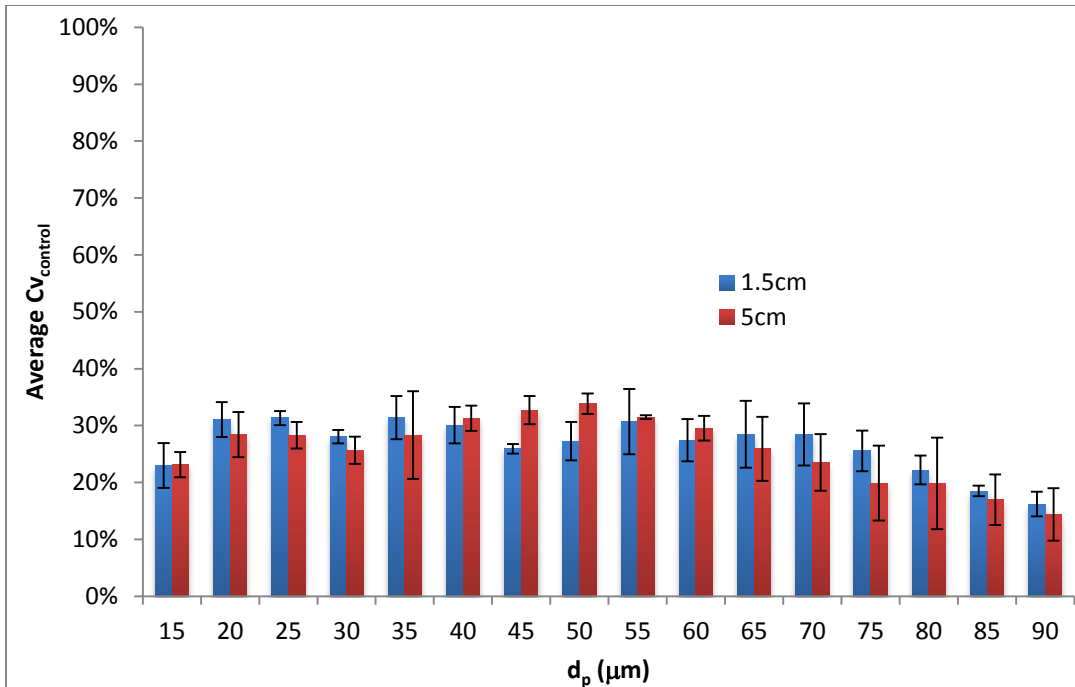


Figure A3: Average $CV_{control}$ per size bin, for 40 μm cut-size tubes.

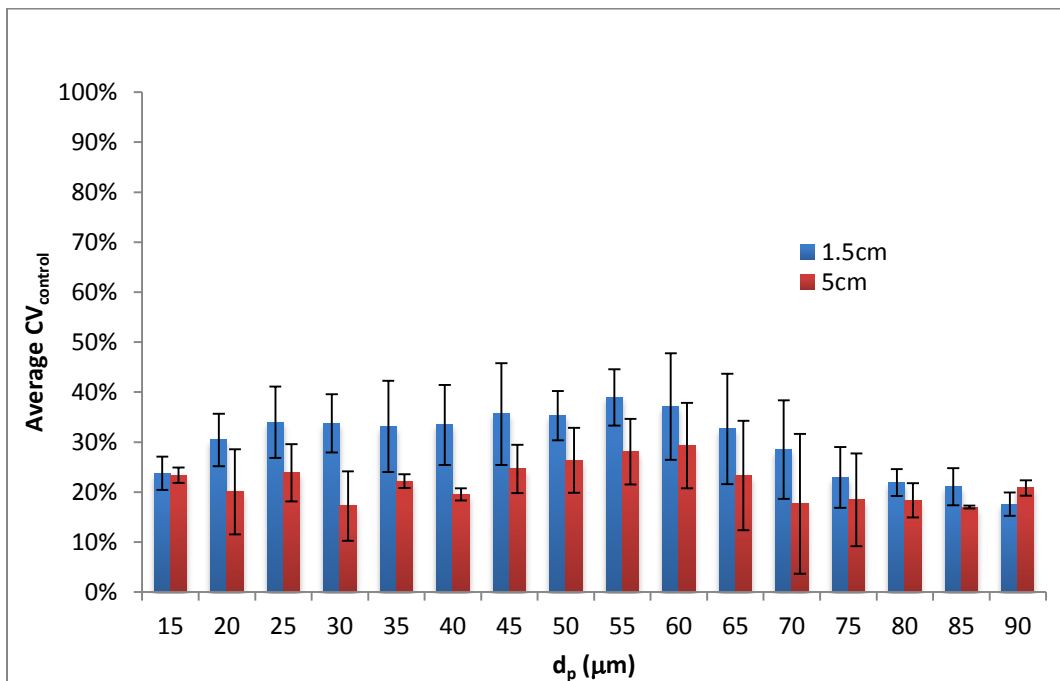


Figure A4: Average $CV_{control}$ per size bin, for 50 μm cut-size tubes.

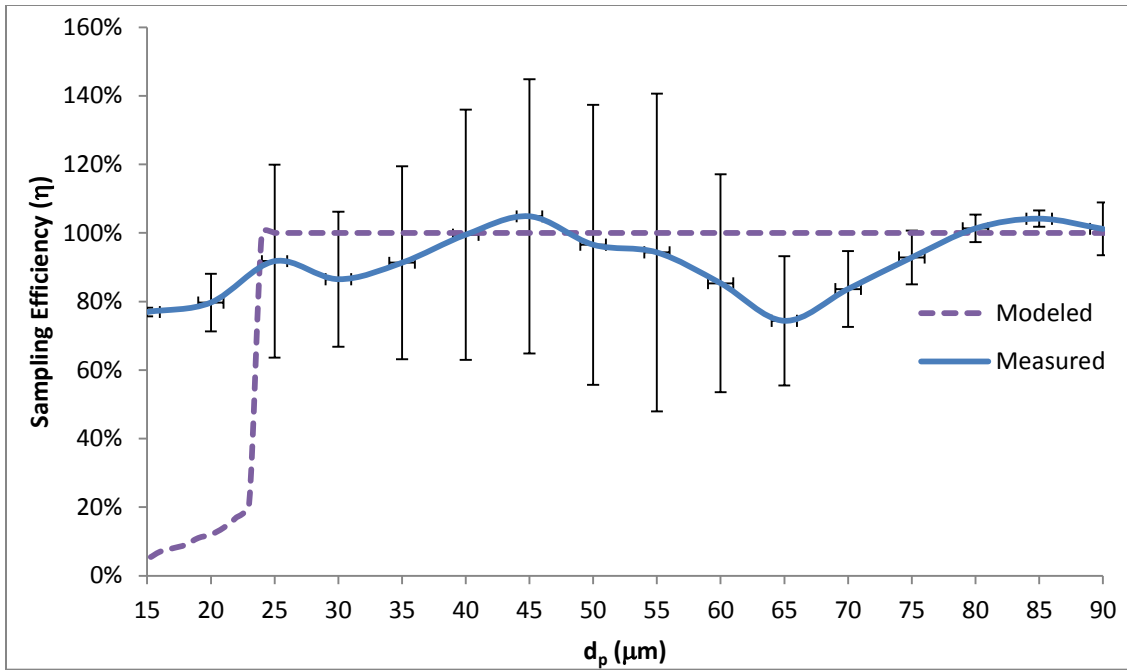


Figure A5: Sampling efficiency for 20 μm cut-size tubes (1.5 cm) based on control filters 1, 4 and 7 only.

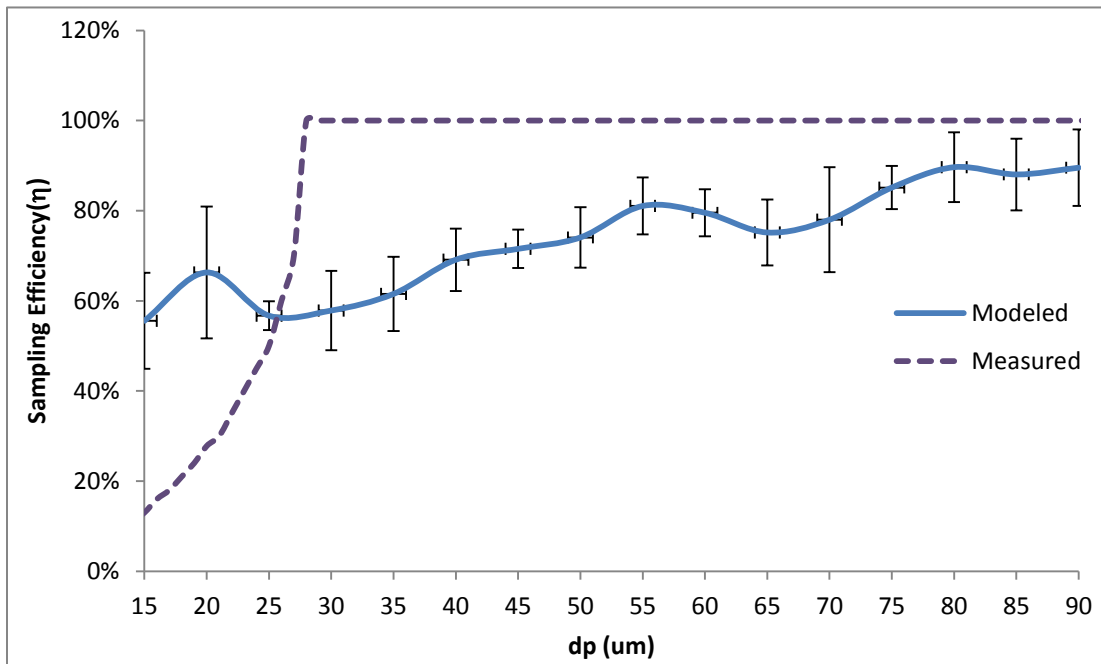


Figure A6: Sampling efficiency for 20 μm cut-size tubes (5 cm) based on control filters 1, 4 and 7 only.

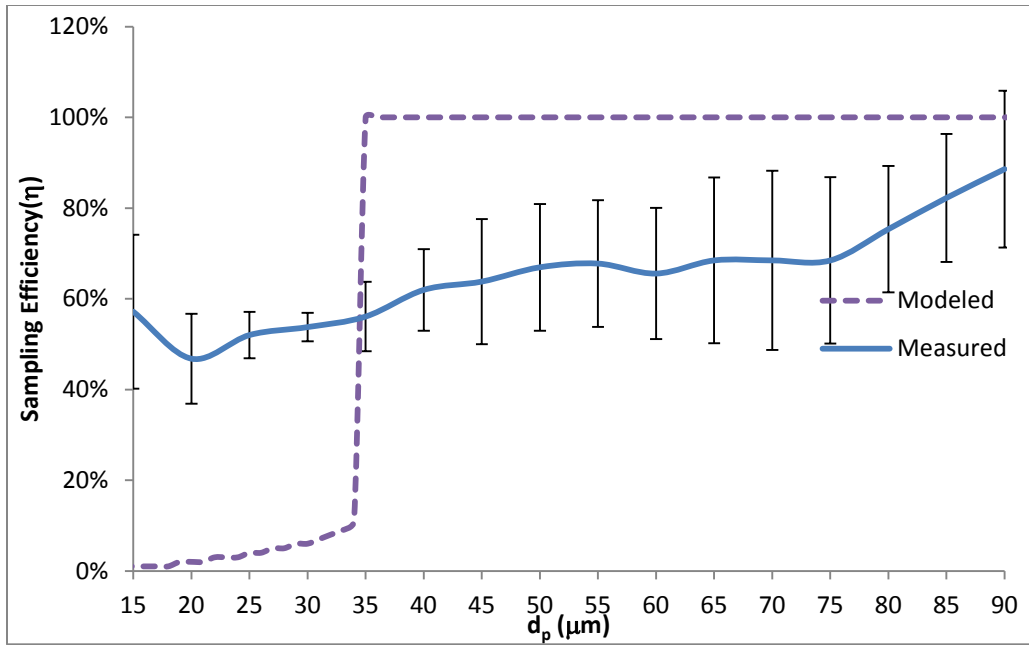


Figure A7: Sampling efficiency for 30 μm cut-size tubes (1.5 cm) based on control filters 1, 4 and 7 only.

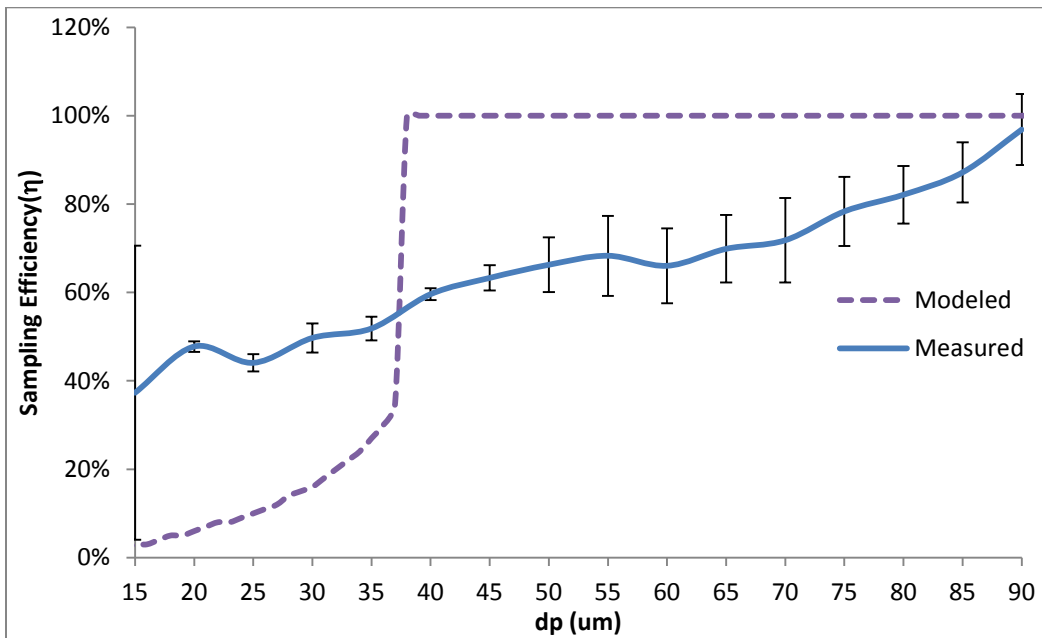


Figure A8: Sampling efficiency for 30 μm cut-size tubes (5 cm) based on control filters 1, 4 and 7 only.

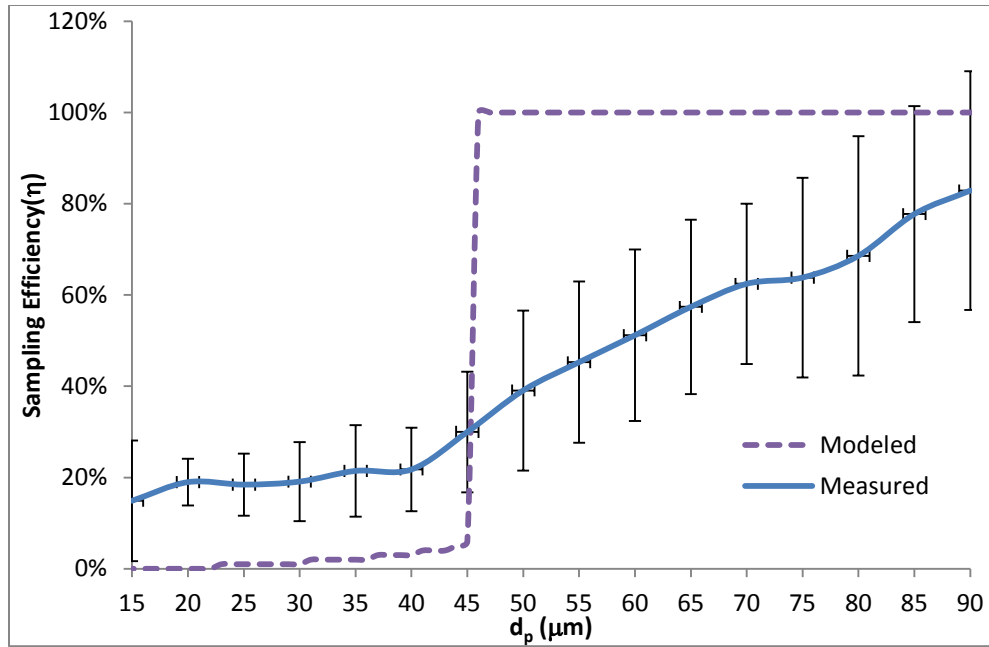


Figure A9: Sampling efficiency for 40 μm cut-size tubes (1.5 cm) using only control filters 1, 4 and 7.

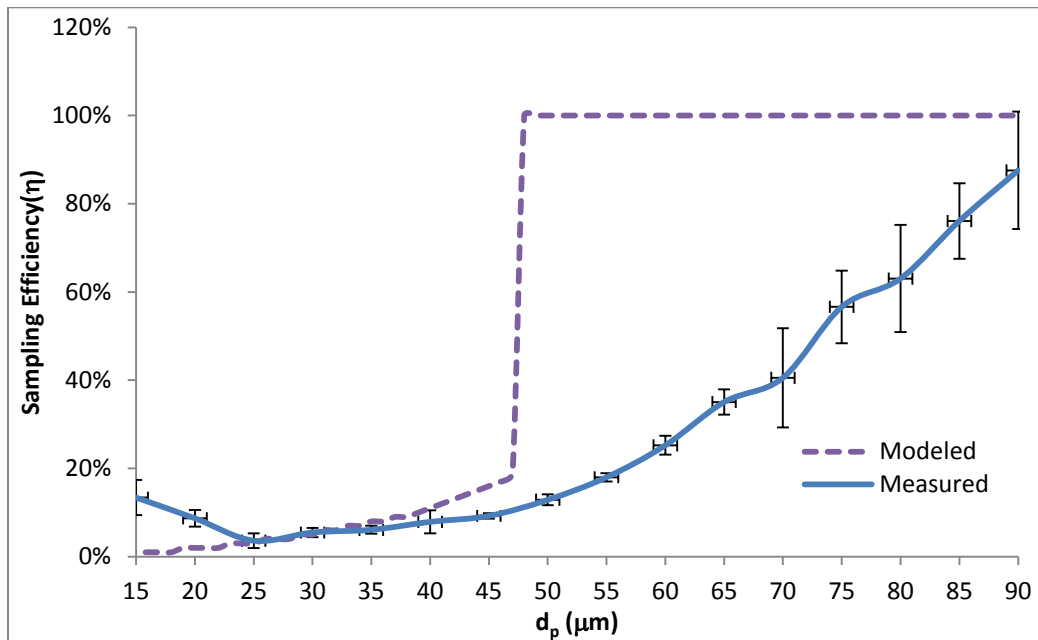


Figure A10: Sampling efficiency for 40 μm cut-size tubes (5 cm) using only control filters 1, 4 and 7.

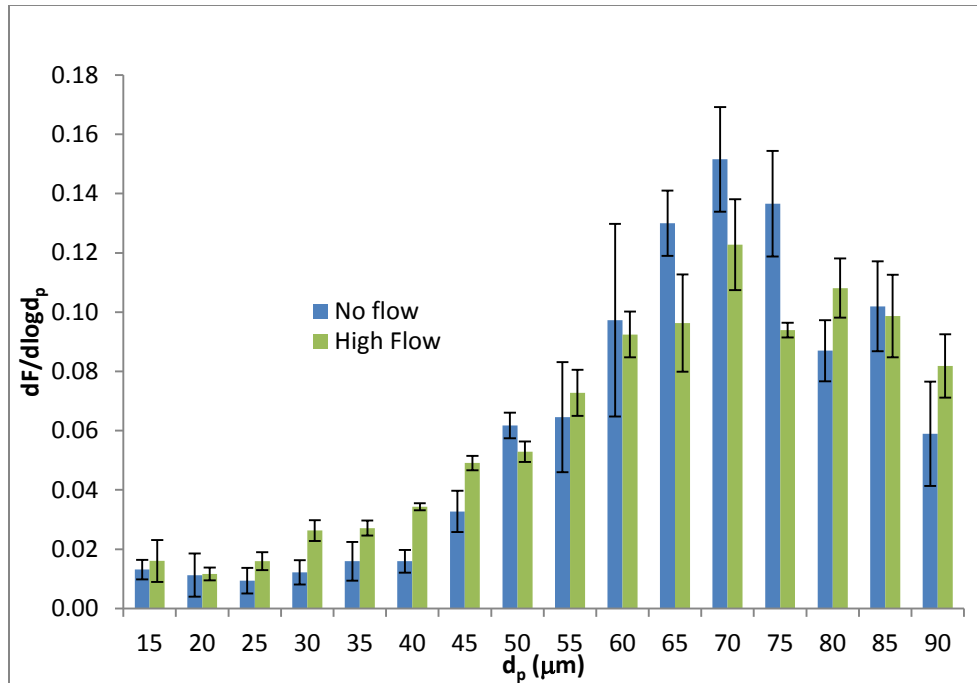


Figure A11: Change in size distribution due to the operating PIPS for control filter

4.

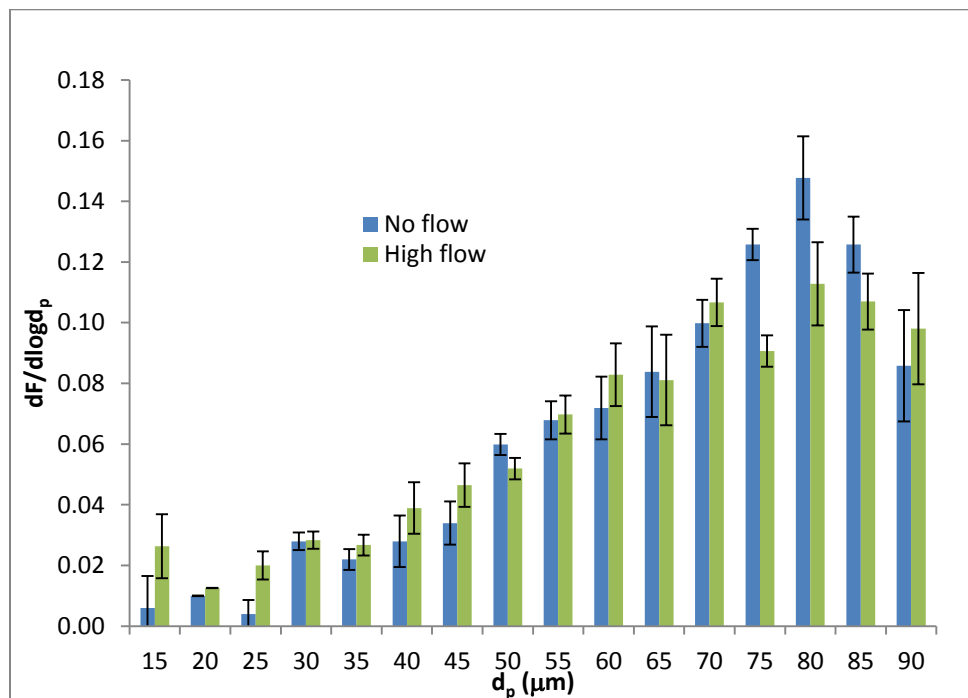


Figure A12: Change in size distribution due to the operating PIPS for control filter 7.

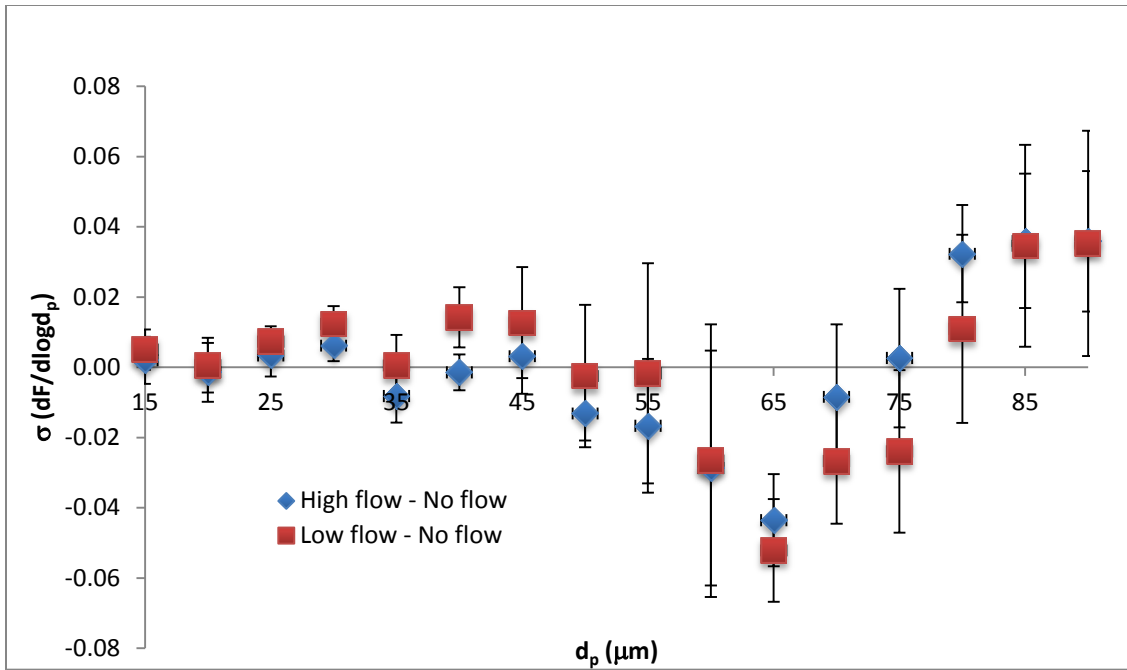


Figure A13: The effect of the high flow PIPS condition on control filter 1 particle deposition.

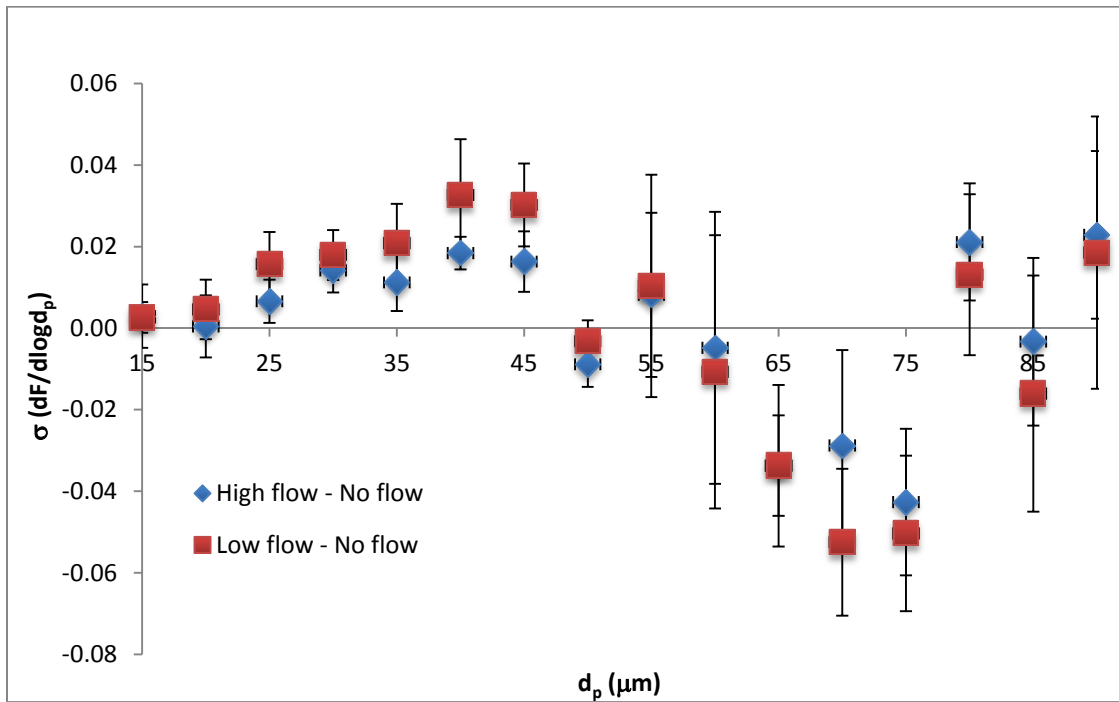


Figure A14: The effect of the high flow PIPS condition on control filter 4 particle deposition.

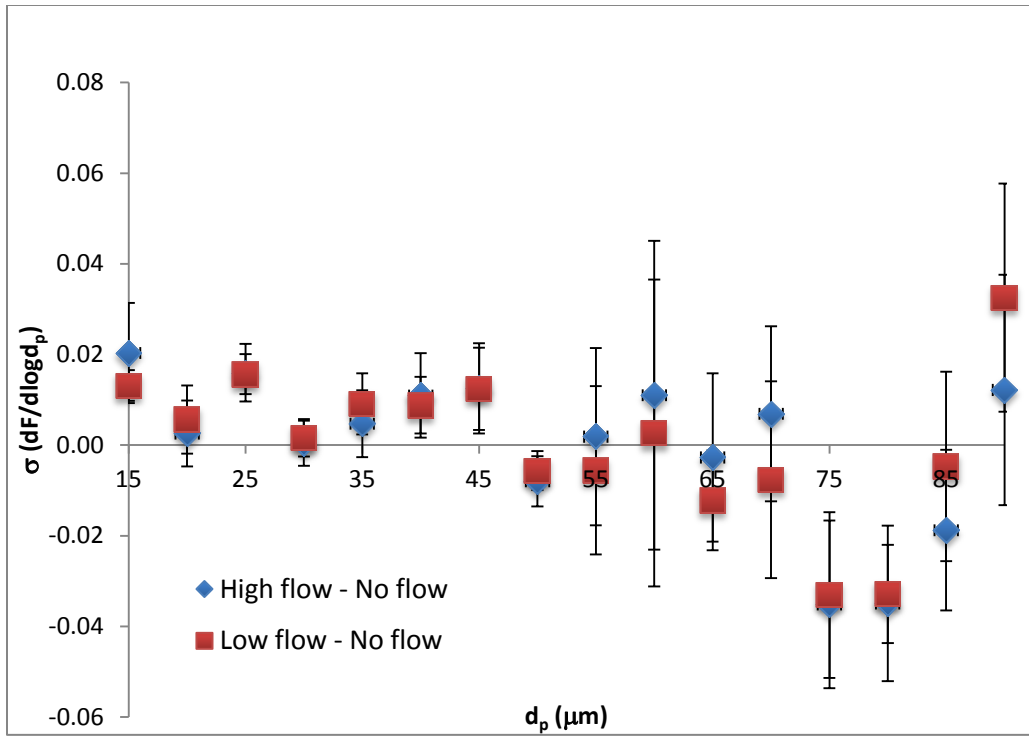


Figure A15: The effect of the high flow PIPS condition on control filter 7 particle deposition.

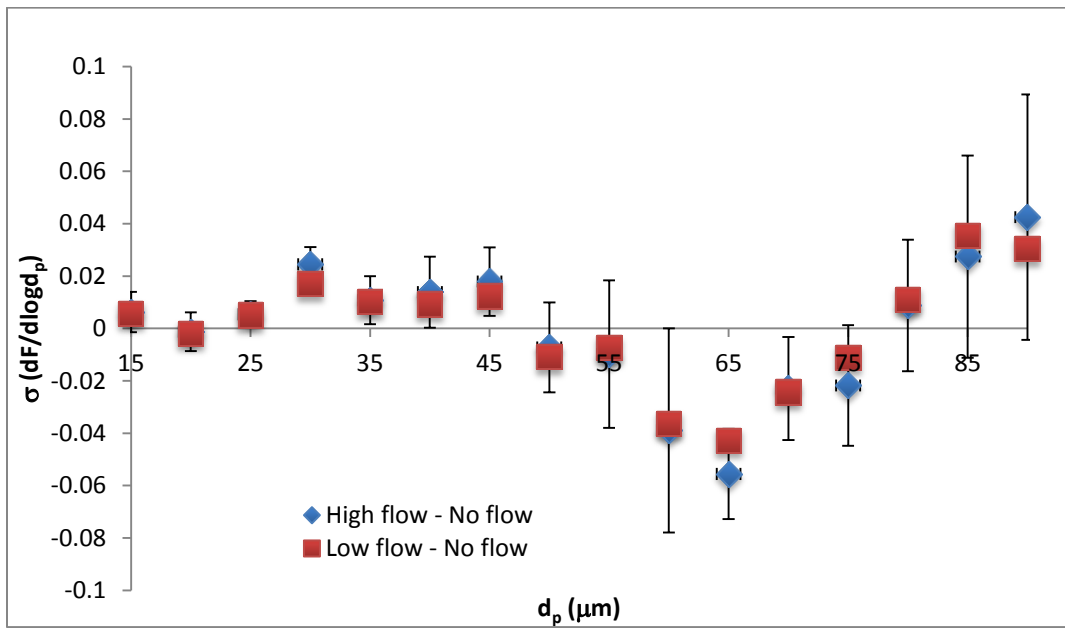


Figure A16: The effect of the high flow PIPS condition on control filter 3 particle deposition.

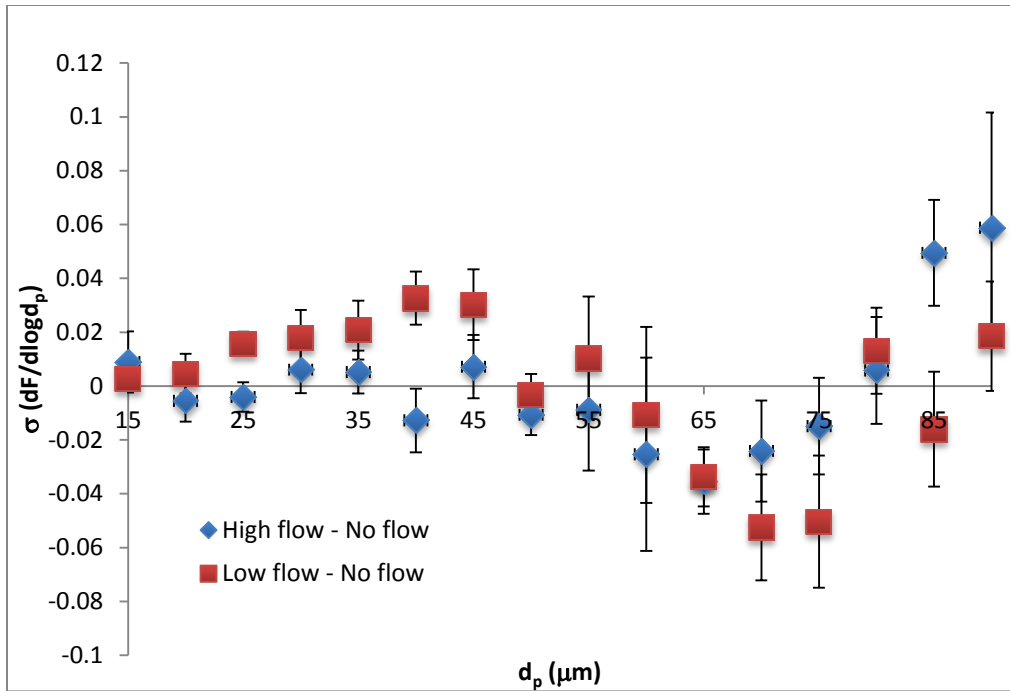


Figure A17: The effect of the high flow PIPS condition on control filter 6 particle deposition.

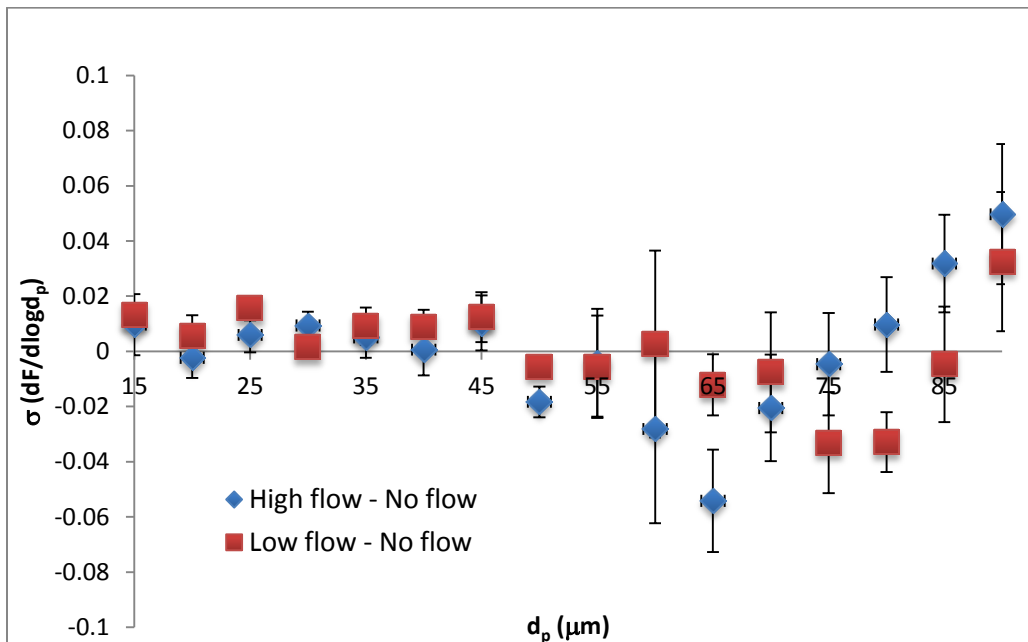


Figure A18: The effect of the high flow PIPS condition on control filter 9 particle deposition.

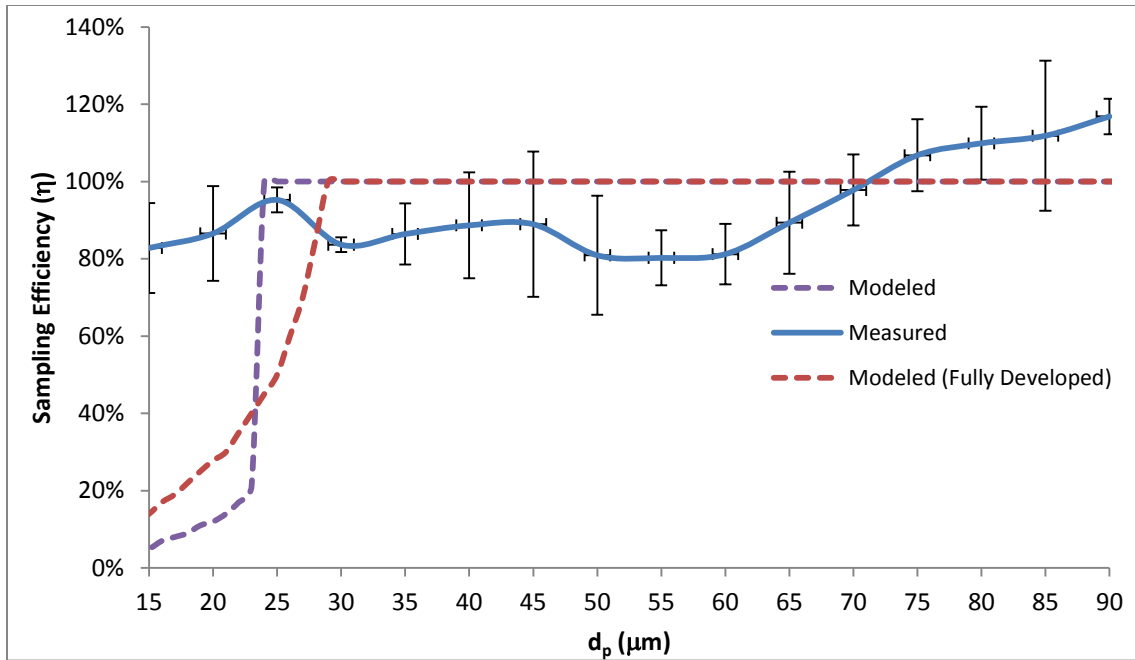


Figure A19: 20 μm cut-size tubes (1.5 cm) compared to developing and fully-developed flow models.

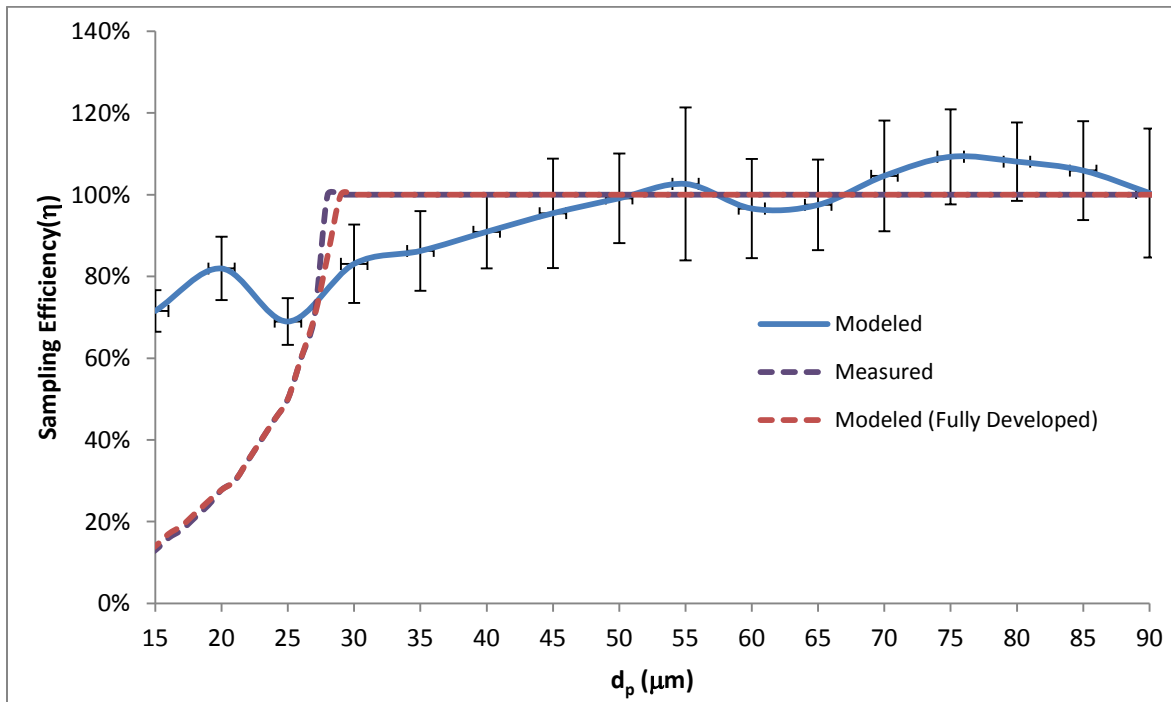


Figure A20: 20 μm cut-size tubes (5 cm) compared to developing and fully-developed flow models.

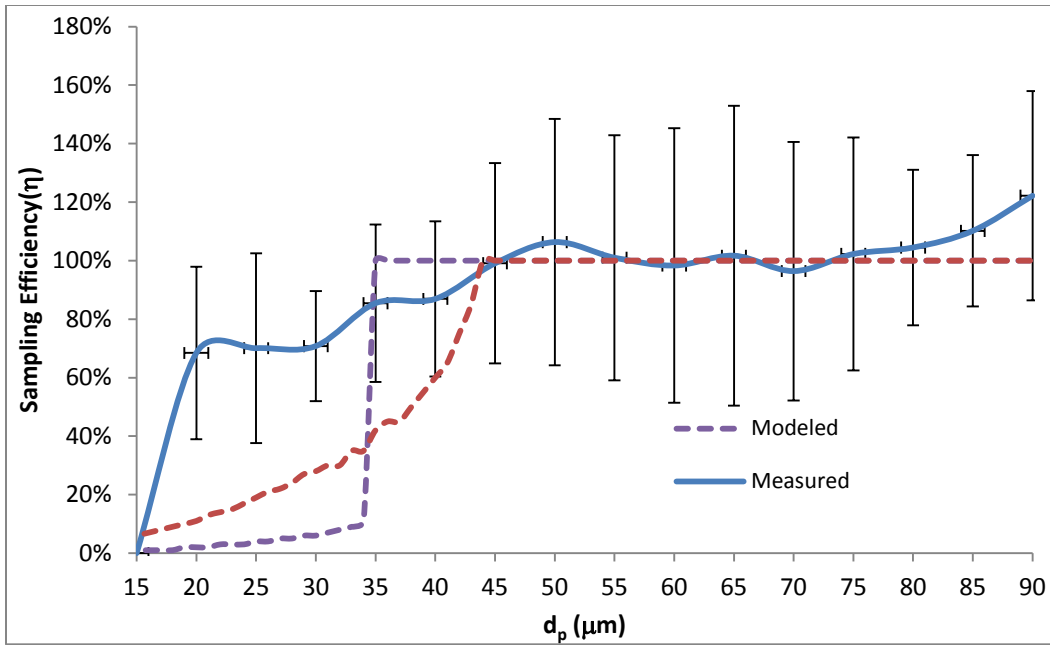


Figure A21: 30 μm cut-size tubes (1.5 cm) compared to developing and fully-developed models.

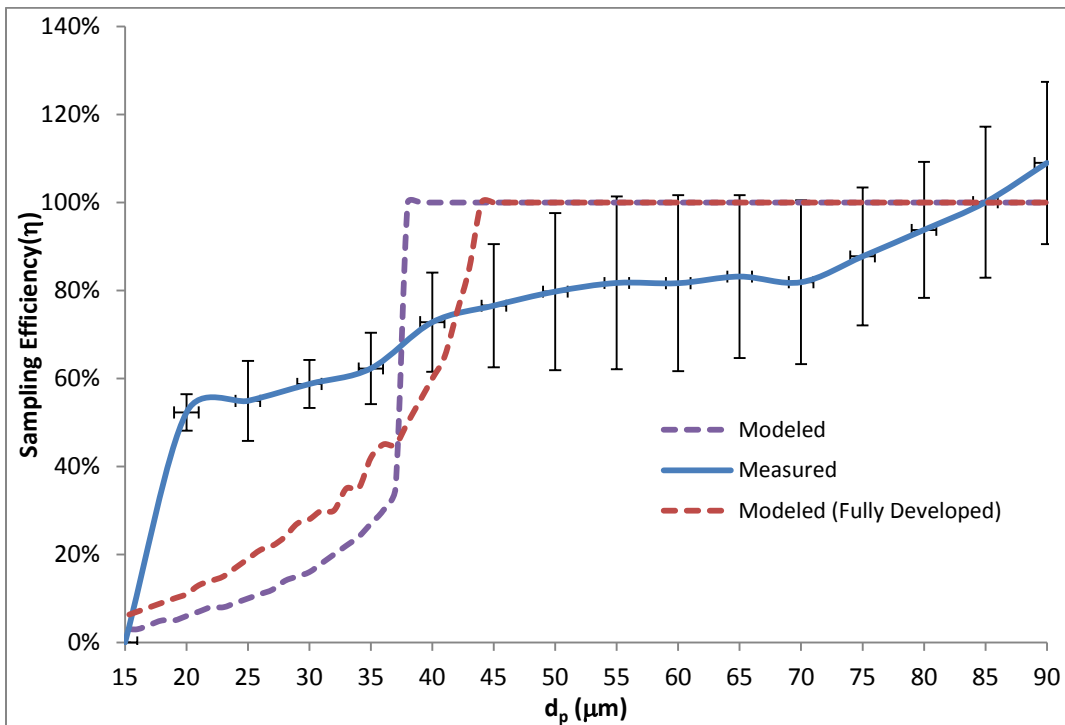


Figure A22: 30 μm cut-size tubes (5 cm) compared to developing and fully-developed models.

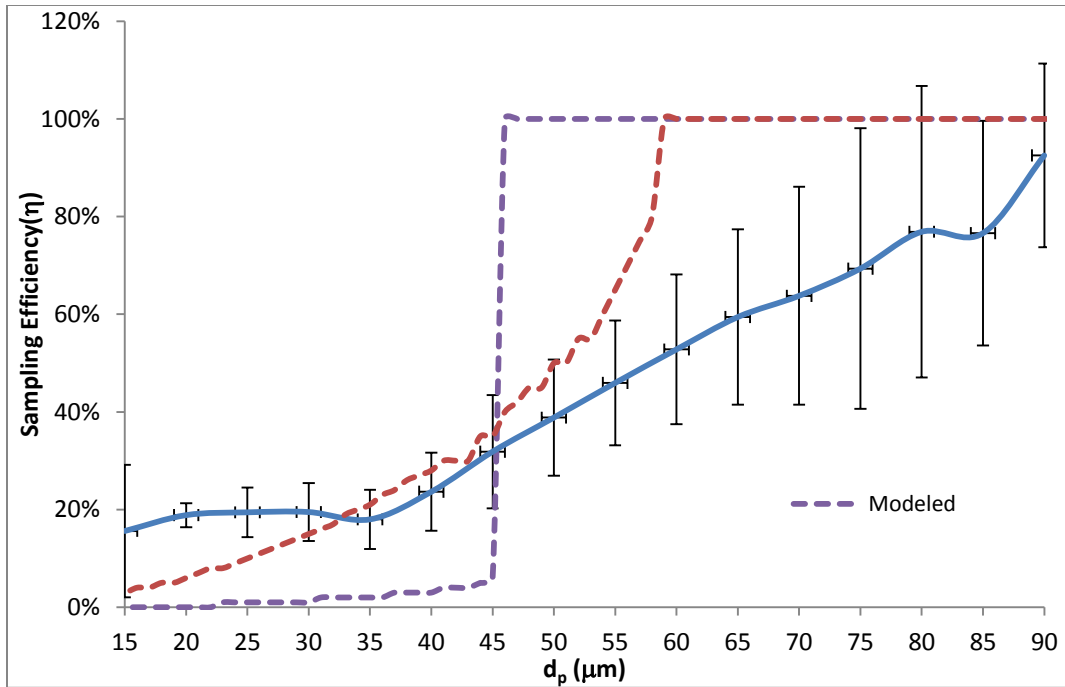


Figure A23: 40 μm cut-size tubes (1.5 cm) compared to developing and fully-developed flow.

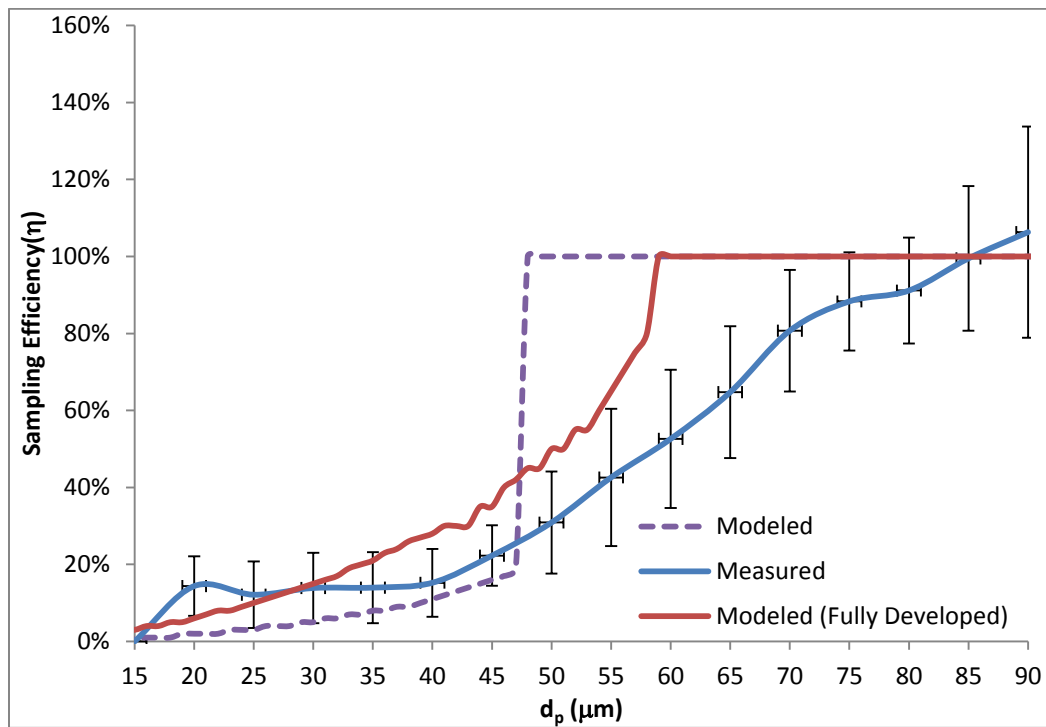


Figure A24: 40 μm cut-size tubes (5 cm) compared to developing and fully-developed flow.

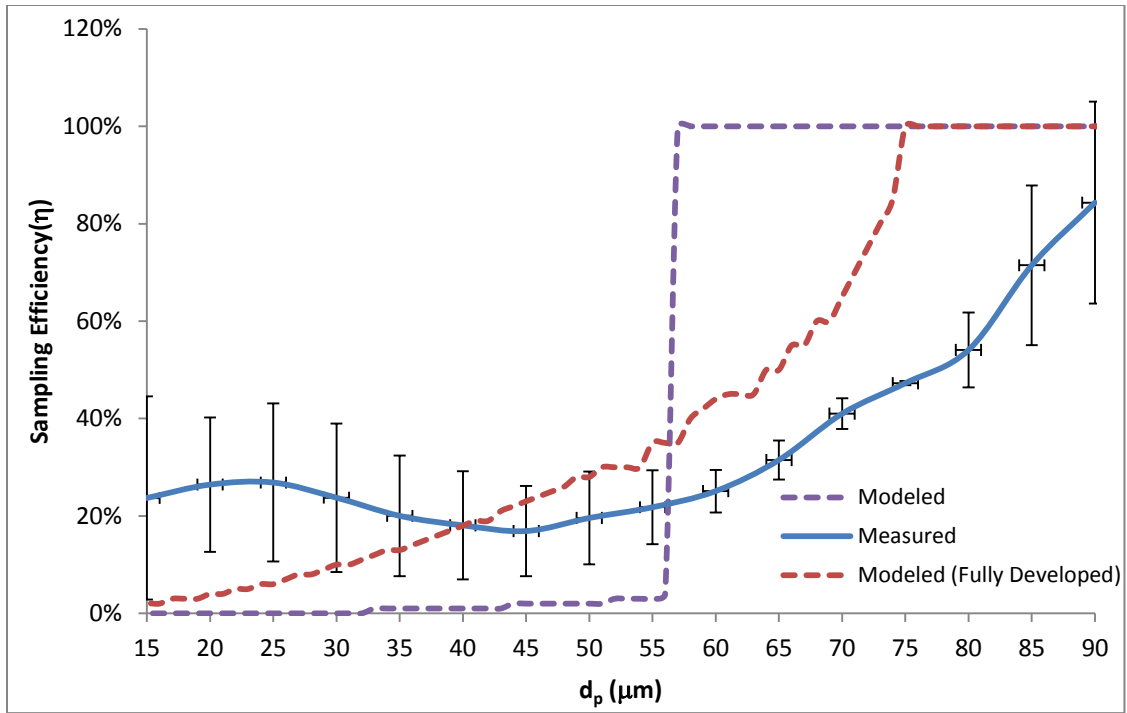


Figure A25: 50 μm cut size tubes (1.5 cm) compared to developing and fully-developed flow.

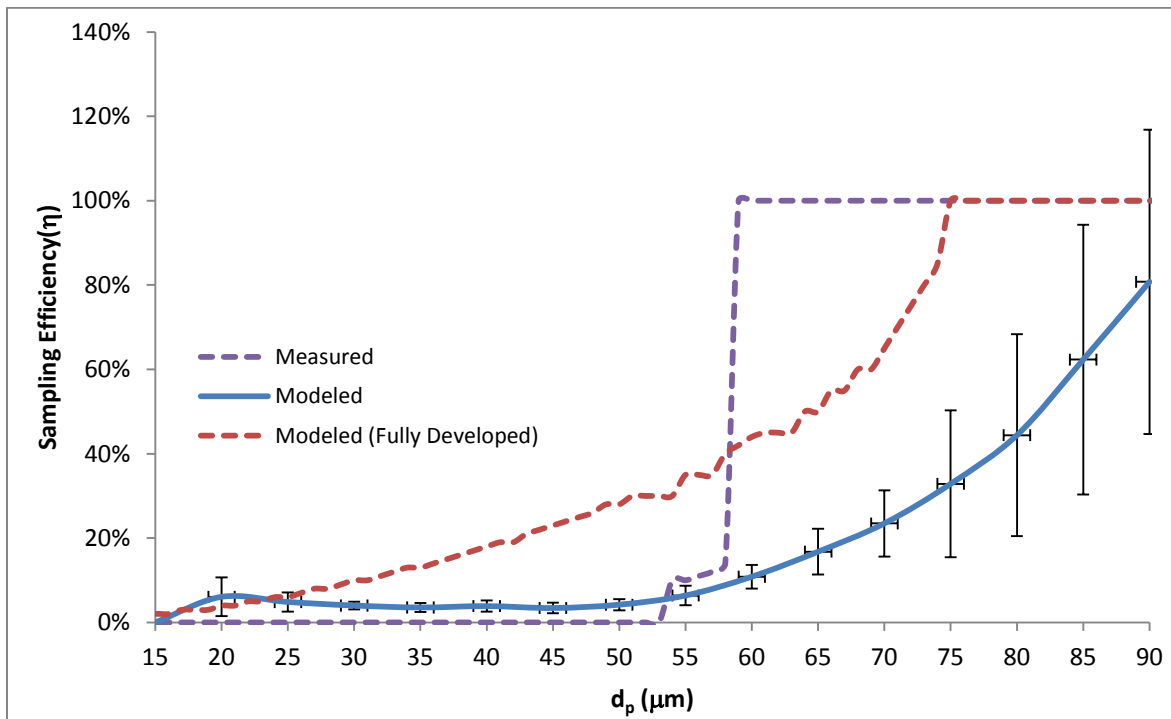


Figure A26: 50 μm cut-size tubes (5 cm) compared to developing and fully-developed flow.